วัสดุความที่มีแข็งแรงสูง: วัสดุเชิงประกอบระหว่างอะลูมินา-เซอร์โคเนียโดยใช้ผงวัตถุดิบราคาถูก

นางสาว กันทิมา เหมรา

วิทยานิพนธ์นี้เป็นส่วนหนึ่งของการศึกษาตามหลักสูตรปริญญาวิทยาศาสตรมหาบัณฑิต
สาขาวิชา เทคโนโลยีเซรามิก ภาควิชาวัสดุศาสตร์
คณะวิทยาศาสตร์ จุฬาลงกรณ์มหาวิทยาลัย
ปีการศึกษา 2546
ISBN: 974-17-4388-2

HIGH STRENGTH MATERIALS: ALUMINA-ZIRCONIA COMPOSITE USING LOW COST RAW POWDER

Miss Khanthima Hemra

A Thesis Submitted in Partial Fulfillment of the Requirements

For the Degree of Master of Science in Ceramic Technology

Department of Materials Science

Faculty of Science

Chulalongkorn University

Academic Year 2003

ISBN: 974-17-4388-2

Thesis Title	High strength materials: Alumina-zirconia composite using low cost raw powder
By	Miss Khanthima Hemra
Field of Study	Ceramic Technology
Thesis Advisor	Chair Professor Shigetaka Wada, Ph.D.
Thesis Co-advisor	Associate Professor Supatra Jinawath, Ph.D.

Accepted by the Faculty of Science, Chulalongkorn University in Partial Fulfillment of the Requirments for the Master's Degree

……Dean of the Faculty of science
(Professor Piamsak Menasveta, Ph.D.)

THESIS COMMITTEE

……Chairman
(Associate Professor Saowaroj Chuayjuljit)

……Thesis Advisor
(Chair Professor Shigetaka Wada, Ph.D.)

……Thesis Co-advisor
(Associate Professor Supatra Jinawath, Ph.D.)

……Member
(Sirithan Jiemsirilers, Ph.D.)

……Member
(Dujreutai Pongkao, Ph.D.)

กันทิมา เหมรา: วัสดุทีมีความแข็งแรงสูง: วัสดุเชิงประกอบระหว่างอะลูมินา-เซอร์โคเนียโดยใช้ผงวัตถุดิบราคาถูก (HIGH STRENGTH MATERIALS: ALUMINA-ZIRCONIA COMPOSITE USING LOW COST RAW POWDER) อ.ที่ปรึกษา: ศ.ดร. ชิเกตากะ วาดะ, อ.ที่ปรึกษาร่วม: รศ.ดร. สุพัตรา จินาวัฒน์, 100 หน้า, ISBN: 974-17-4388-2

วัสดุเซรามิกที่มีความแข็งแรงสูงส่วนใหญ่มักไม่ใช่วัสดุที่มีเฟสเดี่ยว การเติม Yttria-Tetragonal Zirconia Polycrystals (Y-TZP) ลงในอะลูมินาสามารถปรับปรุงความแข็งแรงเชิงกลและความแกร่งของวัสดุเชิงประกอบได้ เนื่องจากเกิดการเปลี่ยนเฟสที่เรียกว่า Transformation toughening นอกจากนี้สมบัติทางกลที่เหนือกว่าวัสดุอื่นนี้ เป็นผลที่เกิดจากกระบวนการผลิตที่พิเศษ เช่น กระบวนการอัดขึ้นรูปโดยใช้ความร้อน (Hot Isostatically Pressed) และใช้วัตถุดิบที่มีขนาดอนุภาคละเอียดมาก งานวิจัยนี้ได้ศึกษาถึงกระบวนการปรับปรุงสมบัติเชิงกลของวัสดุเชิงประกอบระหว่างอะลูมินา-เซอร์โคเนีย โดยใช้ผงวัตถุดิบราคาถูก และกระบวนการผลิตแบบธรรมดา ในการวิจัยได้เลือกใช้ผงอะลูมินา A-21 และผงเซอร์โคเนีย GTYS-5 จากนั้นนำไปผ่านกระบวนการบดเพื่อลดขนาดในแอททริชันมิลล์ และนำผงที่ได้มาผสมในอัตราส่วน A-21/GTYS-5 เป็น 0/100, 20/80, 40/60, 60/40 และ 80/20 เปอร์เซ็นต์โดยน้ำหนัก ขึ้นรูปเป็นชิ้นทดลองโดยการอัด และทำการเผาซินเทอร์ในช่วง 1350-1650 องศาเซลเซียส เป็นเวลา 2 ชั่วโมง

หลังจากผ่านกระบวนการบดเพื่อลดขนาดแล้ว A-21 และ GTYS-5 มีขนาดอนุภาคเฉลี่ยเป็น 0.73 และ 0.57 ไมโครเมตร ตามลำดับ ซึ่งมีแนวโน้มที่สอดคล้องกับพื้นที่ผิวจำเพาะของอนุภาคที่เพิ่มขึ้น และสามารถซินเทอร์ให้มีความหนาแน่นประมาณ 96 ถึง 98 เปอร์เซ็นต์ของค่าทางทฤษฎี เกรนของเซอร์โคเนียมีผลไปยับยั้งการเติบโตของเกรนของอะลูมินาโดยปรากฏที่ขอบเกรนของอะลูมินา เป็นผลให้วัสดุเชิงประกอบมีขนาดเกรนลดลงเมื่อปริมาณ GTYS-5 เพิ่มขึ้น ความแข็งของวัสดุเชิงประกอบมีแนวโน้มเพิ่มขึ้นเมื่อปริมาณ A-21 เพิ่มขึ้น ความแกร่งของวัสดุเชิงประกอบมีค่าสูงสุด 6.0 $MPa.m^{1/2}$ เมื่อมีปริมาณ GTYS-5 เป็น 20 และ 80 เปอร์เซ็นต์โดยน้ำหนัก ชิ้นตัวอย่างที่มี GTYS-5 เป็น 80 เปอร์เซ็นต์โดยน้ำหนักมีค่าความแข็งแรงดัดถึง 632 เมกะปาสคาล เมื่อปริมาณ GTYS-5 ที่สูง กลไกหลักในการแตกหักของวัสดุเชิงประกอบเกิดจากการเปลี่ยนเฟสจากเตตระโกนอลเป็นโมโนคลินิกที่เรียกว่า t→m transformaton เป็นผลให้วัสดุแตกผ่านเกรน

ภาควิชาวัสดุศาสตร์ ลายมือชื่อนิสิต.....
สาขาวิชา เทคโนโลยีเซรามิก ลายมือชื่ออาจารย์ที่ปรึกษา.....
ปีการศึกษา 2546 ลายมือชื่ออาจารย์ที่ปรึกษาร่วม.....

4472522623 : MAJOR CERAMIC TECHNOLOGY

KEY WORD : ALUMINA-ZIRCONIA COMPOSITE/STRENGTH/ TOUGHNESS/ TRANSFORMATION TOUGHENING

KHANTHIMA HEMRA: HIGH STRENGTH MATERIALS: ALUMINA-ZIRCONIA COMPOSITE USING LOW COST RAW POWDER, THESIS ADVISOR: PROF. SHIGETAKA WADA, Ph.D., THESIS CO-ADVISOR: ASSOC. PROF. SUPATRA JINAWATH, Ph.D., 100 pp., ISBN: 974-17-4388-2

Most of high performance ceramics are not single-phase materials. The addition of Yttria-Tetragonal Zirconia Polycrystals (Y-TZP) to alumina can improve strength and toughness of the composites through a phenomenon known as transformation toughening. Moreover, their superior mechanical properties are achieved by special process such as hot isostatically pressed (HIP), and using fine particle material. This research focuses on using low cost raw powders and non-special process. In order to know the effect of ZrO_2/Al_2O_3 ratio on the mechanical properties, Al_2O_3 A–21 and ZrO_2 GTYS-5 were used as raw powders and the attrition mill was used to reduce the particle size of these powders. The compositions of Al_2O_3 (A)-ZrO_2 (Z) specimens were 100A, 80A20Z, 60A40Z, 40A60Z, 20A80Z, and 100Z. They were prepared by ball mill mixing and sintered at a temperature ranging from 1350-1650^{O}C for 2 hours.

The particle sizes of A-21 and GTYS-5 at 50wt% cumulative (D_{50}) were 0.73 and 0.57 μm, respectively. The tendency of particle size distribution change corresponded to the increment of specific surface area. Those milled powders could be sintered to nearly theoretical density (96-98%). The average grain size of A-21 decreased with increasing GTYS-5 content. The ZrO_2 predominantly at the grain boundary of Al_2O_3 effectively pinned the grain growth of Al_2O_3 and limited the Al_2O_3 grain size. Therefore, Vickers hardness (H_v) of the composite increased with increasing A-21 content. Fracture toughness (K_{1c}) of 80A20Z and 20A80Z was maximum at 6.0 MPa.m$^{1/2}$. The flexural strength of 20A80Z (632 MPa) was higher than 80A20Z (525 MPa). The t→m transformation was thought to be the main mechanism to increase $K_{1c}$and the transgranular fracture found in the composites containing high GTYS-5 content suggested the high strength.

Department Materials Science — Student's signature……..

Field of study Ceramic Technology — Advisor's signature……

Academic year 2003 — Co-advisor's signature……

Acknowledgements

I would like to express my sincere gratitude to my advisor, Professor Dr. Shigetaka Wada, for his encouragement, suggestion, and for all that I have learnt from him throughout this research. His advice inspired the good idea and motivated the research to be completed. I would like to extend my gratitude to my co-advisor, Associated Professor Dr. Supatra Jinawath, who gave me a good advice and my research would not be completed without her invaluable suggestions.

I would like to thank the Graduate School of Chulalongkorn University and the MEIDEN Ceramics Corporation for the research financial support.

Thanks to all my friends at the Department of Materials Science for their friendship and assistance.

I would like to express my gratitude to my family for their love, understanding, and encouragement. Finally, I would like to dedicate my success to my brother. Although he is not alive, still he is always in my mind.

CONTENTS

CONTENTS (cont.)

CONTENTS (cont.)

LIST OF TABLES

LIST OF FIGURES

LIST OF FIGURES (cont.)

Page

CHAPTER 1

INTRODUCTION

1.1 Introduction

Alumina is a popular ceramic material for structural applications. The important role of this material is to support mechanical loading. Thus, the high mechanical behaviors are obtained by using appropriate fabrication and raw materials. However, most ceramic materials are brittle. Transformation toughening is one of the best methods to improve their fracture toughness and strength. Among this transformation, toughened ceramic materials, alumina-zirconia ceramic composites have been studied widely.

Generally, most high performance ceramics are not single-phase materials. Alumina-zirconia ceramic composite is a class of high strength and high toughness structural material. Their superior mechanical properties such as high strength, high toughness, good wear resistance and good corrosion resistance are achieved through various special processes and by using very fine particles. The average bending strength of 2.4 GPa for a composite that containing 20 wt% Al_2O_3-ZrO_2 [1] is obtained, when using the submicrometer composite powder, Sumitomo- Al_2O_3 and TSK- ZrO_2, isostatically cold pressed at 300 MPa and sintered at 1500 ^{O}C to full density followed by hot isostatic press at 1500 ^{O}C and 100 MPa for 0.5 h.

It has been desired that alumina-zirconia ceramic composites can be extended to more structural works [2]. One of the applications is ceramic insert, Fig.1.1, which is used in many construction works such as marine tunnel construction work, Fig.1.2 (a), the moored ships, Fig.1.2 (b), underground utility tunnels, Fig.1.2 (c), and tunnel construction work, Fig.1.2 (d). The product is made of a high-purity alumina ceramic material; however, the addition of yttria-tetragonal zirconia to alumina improves fracture toughness that can increase the component life

and performance. So far these materials have not been successfully commercialized due to too expensive cost of starting materials and complicated fabrication.

From this point of view, fabricating materials with high mechanical strength using cheaper starting powders and simple process can solve this problem provided that mechanical strength is attained.

1.2 The objectives of this research are:

1. To achieve the bending strength of alumina-zirconia ceramic composites to the target value of 1 GPa.
2. To reduce the production cost by using low-cost raw powders and non-special processes.

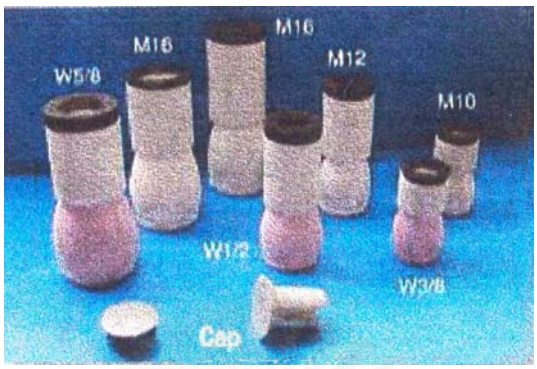

Fig.1.1 Ceramic insert [3]

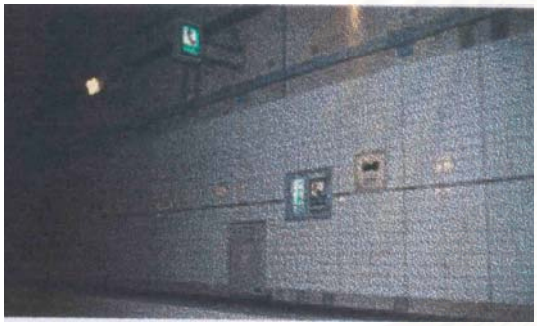

(a)

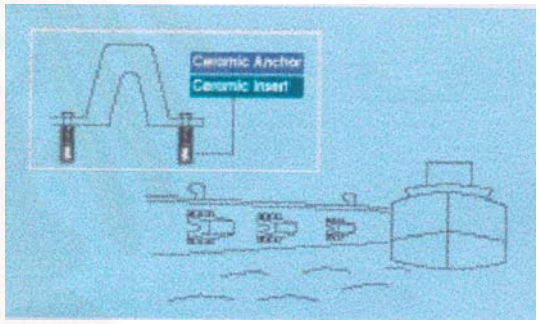

(b)

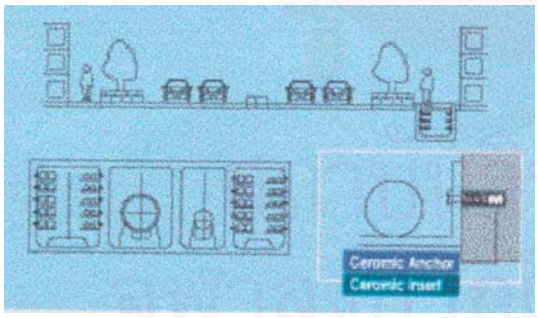

(c)

(d)

Fig.1.2 Application of ceramic inserts in many constructions works (a) marine tunnel, (b) the moored ship, (c) underground utility, and (d) tunnel construction work [2]

CHAPTER 2

LITERATURE REVIEWS

2.1 Zirconia Ceramic

2.1.1 Zirconia Resources

In nature, Zirconium compounds are found as zircon ($ZrSiO_4$) and baddeleyite (ZrO_2) [4]. The average content of zirconia in baddeleyite is 80%-90%. It can be used for many purposes i.e. as refractory materials without any further purifying [5]. Zirconia can be prepared from many processes such as chemical and plasma process [4].

In chemical processes, the undesirable elements are removed by using (i) chlorination and thermal decomposition, (ii) alkali oxide decomposition and (iii) lime fusion.

(i) Chlorination and thermal decomposition: A high purity grade of zirconia can be obtained by mixing zircon with carbon in an amount enough to wrap the total oxygen of the ore and heating up to 800 – 1200^{O}C.

$$ZrO_2.SiO_2 + C + 4Cl_2 \longrightarrow ZrCl_4 + SiCl_4 + 4CO$$

The chlorination is initiated when chlorine gas get into the mixture and form zirconium tetrachloride. The major impurities are the chloride of iron, titanium, aluminium, and silicon but all chlorides formed are volatile. Then, they are refined out at 150-180^{O}C. Hydrolysis with water of soluble chlorides produces a solution of zirconium oxychloride. Next, the solution is cooled down and zirconium oxychloride is precipitated. The oxychloride is separated by reaction with concentrated hydrochloric acid and the crystals are calcined to

zirconium oxide or dissolved in water and precipitated with ammonia as zirconium oxide hydrate. After calcination, a pure white zirconia powder is produced.

(ii) Alkali oxide decomposition is the method to fuse zircon ore with sodium hydroxide at 600^{O}C, to form a mixture of sodium zirconate with sodium silicate.

$$ZrO_2.SiO_2 + 4\ NaOH \longrightarrow Na_2ZrO_3 + Na_2SiO_3 + 2H_2O$$

The mixture is leached with water to remove sodium silicate and retained as the hydrolysed zirconate. The precipitate is filtered and treated with sulfuric acid to produce zirconyl sulphate. The solution is diluted and precipitated in ammonia. The calcination is used to yield zirconia powder.

(iii) Lime fusion is the process that calcia is added to zircon and the mixture is heated to 1100-1600^{O}C.

$$2CaO + ZrO_2.SiO_2 \xrightarrow{1600^{O}C} ZrO_2 + CaSiO_4$$

The various mixtures of zirconium oxide and calcium silicate are produced. The mixture is leached with hydrochloric acid to remove the calcium silicate. Then it is washed and dried to obtain zirconia powder.

In the plasma process [6], the zircon sand is heated in plasma arc. It melts and dissociates into the component ZrO_2 and SiO_2, when injecting into an arc. The physical and chemical properties of the final zirconia powder can be controlled by controlling the condition of plasma arc.

Pure zirconia is monoclinic structure at room temperature. Zirconia always contains 2% of hafnium oxide and is contaminated with silica, titanium oxide, iron oxide and so on.

2.1.2 Structure of Zirconia

Zirconia ceramics have been researched for many years. It is an attractive material for high temperature application because of its high melting temperature (2680^{O}C) and excellent corrosion resistance [7]. It shows the polymorphs that are different in crystal structure but of the same chemical composition [8]. Three crystallographic forms, monoclinic, tetragonal, and cubic are found when the temperature is changed [9].

$$\text{Monoclinic} \xrightarrow[1170^{O}C]{} \text{tetragonal} \xrightarrow[2370^{O}C]{} \text{cubic} \xrightarrow[2680^{O}C]{} \text{liquid}$$

The monoclinic phase (m-ZrO_2) is stable at low-temperature until 1170^{O}C, and it changes to the tetragonal phase (t-ZrO_2). The tetragonal phase is stable to 2370^{O}C and the cubic phase (c-ZrO_2) of fluorite type [5] becomes stable at above this temperature till the melting point of 2680^{O}C.

By X-ray analysis, zirconia has a crystallographic changing with temperature [4] as shown in Table 2.1

Table 2.1 Lattice constants of three zirconia crystals [4].

Lattice constants	Crystal structures		
	Monoclinic	Tetragonal	Cubic
a (Å)	5.174	5.07	5.1
b (Å)	5.266	5.07	5.1
c (Å)	5.308	5.16	5.1
α(deg.)	90	90	90
γ (deg.)	90	90	90
β (deg.)	80.8	90	90

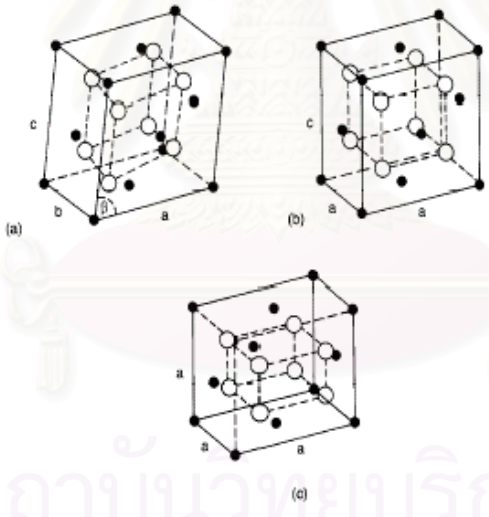

Fig.2.1 Zirconia exists in 3 different crystal structures, ● is zirconium atom, and O is oxygen atom (a) monoclinic at low temperature, (b) tetragonal at intermediate temperature, (c) cubic at high temperature [10].

Firing pure zirconia cannot produce strong pieces of sintered body [5] because the displacive tetragonal-monoclinic (t⟶m) phase transformation occurs. By the transformation, structure distorts, bond angles change but it is not breaking and occurs rapidly as the temperature changes [8].

The tetragonal-monoclinic (t→m) phase transformation is accompanied by volume expansion of ~4%. This change of volume in transformation can result in the failure of component, decreasing the Young modulus and the strength, furthermore the fabrication of components are unreliable. Thus, at the beginning, the application of zirconia ceramic was limited to refractory [7]. However, ZrO_2 has good properties such as hardness, wear resistance, elastic modulus, chemical inertness, low thermal conductivity, high melting temperature, thus there have been desires to improve its mechanical properties for various engineering applications [11]. The example of property data of high purity zirconia (ZrO_2 TOSO TZ-3YSB-E) is shown in Table 2.2 [12].

Table 2.2 Chemical compositions and properties of ZrO_2 TOSO TZ-3YSB-E.

Chemical compositions and Properties		Quantitative data
Density		6.07g/cc (Archimedes' method)
Fracture toughness		5.0MPa.$m^{1/2}$ (SEPB method, JIS R1607)
Bending strength		1100MPa (4-point bending method at room temperature, JIS R1601)
Hardness		13.00 (HV10, 10 kgf, JIS R1610)
Thermal conductivity		3.1W/mK (JIS R1611)
Thermal expansion		11.1 x10^{-6}/ °C (at 20°C – 100°C, JIS R1618)
Chemical composition	$ZrO_2 + HfO_2$	> 94.0
	Y_2O_3	< 5.65
	Al_2O_3	< 0.30
	SiO_2	< 0.02
	Fe_2O_3	< 0.01
	Na_2O	< 0.04

2.1.3 The Tetragonal-Monoclinic Transformation

Zirconia can be used with its full efficiency by controls the t→m phase transformation using a modifier such as MgO, CaO, CeO_2, and Y_2O_3 [13] as a stabilizer. It can improve strength and toughness when the suitable element added in amounts sufficient to suppress this phenomenon.

The t→m transformation occurs at ~1000^{O}C, the thermal cycling through the transformation range (800↔1200^{O}C) [14] causes the occurring of the spontaneous transformation [15]. The tetragonal phase can be stable until the temperature decreases to room temperature by controlling the stabilizer in this phase. However, ZrO_2 particles can undergo the t→m transformation in the stress field of advancing cracks [16] that will be described in section 2.1.4.

The characteristic of transformation in zirconia is athermal, diffusionless and concerns with atomic movement at the same time, so results in shape change of the transformed region [17].

The transformation is diffusionless that is absence of diffusion. The atoms move in an organized manner relative to their neighbors and forms rapidly, diffusion is not required. Thus, the reaction does have not chemical composition change [15].

The change of shape is the displacive transformation, a lattice distortion, and resulting in a large strain. Such that the product phase shears from the parent phase, but remains necessary coherent with the parent phase which they are connected by the habit plane. The habit plane is an invariant plane, undistorted and unrotated during the transformation.

The invariant plane strain IPS (the shape strain S), a strain which the parent and product phases leave the habit plane, composes of an expansion or contraction (ξ) normal to the invariant plane together with a shear (γ) that illustrated in Fig.2.2 and associated with the volume change (ΔV)

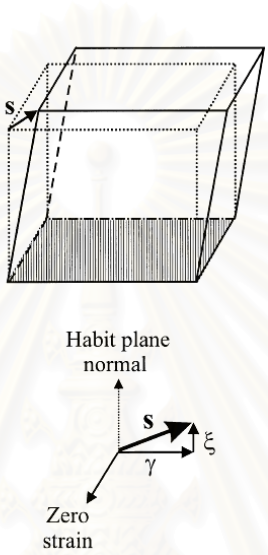

Fig.2.2 Invariant plane strain S, composed of shear component γ parallel to the habit plane (shaded) and an expansion or contraction ξ (=ΔV) normal to the habit plane. Note that the strain is zero in the direction perpendicular to S and to habit plane normal.

In general, the conversion of structure of parent phase to product phase requires overall strain S and another strain that is Bain strain B. The Bain strain must not alter the crystal structure of the new product phase, but must change the shape of the transformed volume in the way from the condition of IPS.

In addition, the strain that combines with the Bain strain produces an undistorted plane is known as the lattice invariant shear LIS. It can occur by either slip or twinning, the improper interface at the parent and product phases is appeared repeatedly relieved by the twinned or slipped lamellas, but in macroscopic scale the interface is approximately undistorted [11, 15].

Finally, a rotation of the transformed lattice R will be required to recognize that the undistorted plane is also unrotated.

The strain of transformation can be illustrated schematically as shown in Fig.2.3.

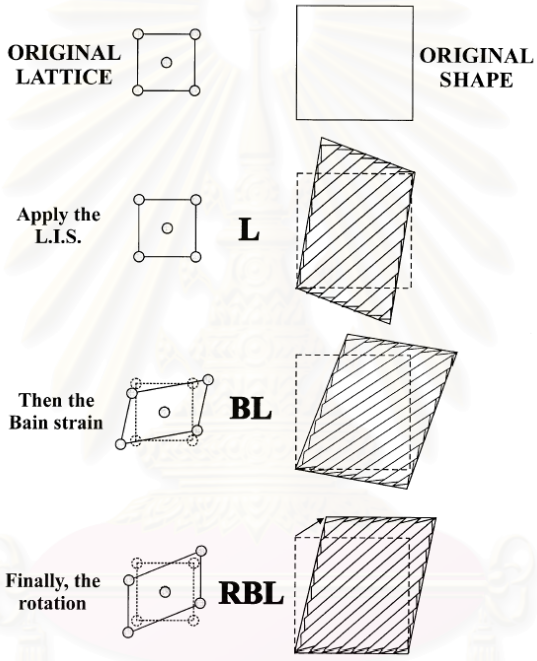

Fig.2.3 Schematic illustration of the steps involved in the phenomenological theory of t→m transformation. The changes to the crystal structure are shown on the left and to the macroscopic transforming volume on the right [17].

2.1.4 Transformation Toughening

In pure zirconia, the tetragonal phase transform to the monoclinic form during cooling. The transformation of tetragonal (t) to monoclinic (m) zirconia has been widely used to increase the toughness of ceramic materials.

By the transformation toughening mechanism, fracture toughness (K_{1c}) increases to 3.0 - 15.0 MPa.$m^{1/2}$ [9]. A variety of ceramics have been used as the ceramic matrix such as Al_2O_3 that is used in this research. When a composite of ZrO_2 / other ceramic is cooled below the transformation temperature, the ZrO_2 tends to expand by t→m transformation. However, this expansion is against by the high stress of the surrounding matrix, therefore, the tetragonal form is retained at room temperature. Hence, the residual stress and energy in each tetragonal zirconia precipitate want to be released.

If a crack is formed in the ceramic, tetragonal precipitates at the crack tip are able to expand and transform to the stable monoclinic form. This mechanism suppresses the crack propagation and raising both toughness and strength.

The transformation material can be separated into two groups as follows:

(i) The tetragonal phase retains in ceramics before damaged. Transformation toughening mechanism enhances the toughness. (Fig.2.4)

(ii) The monoclinic phase precipitates in ceramics before damaged. Microcracking mechanism causing enhanced toughness. (Fig.2.5)

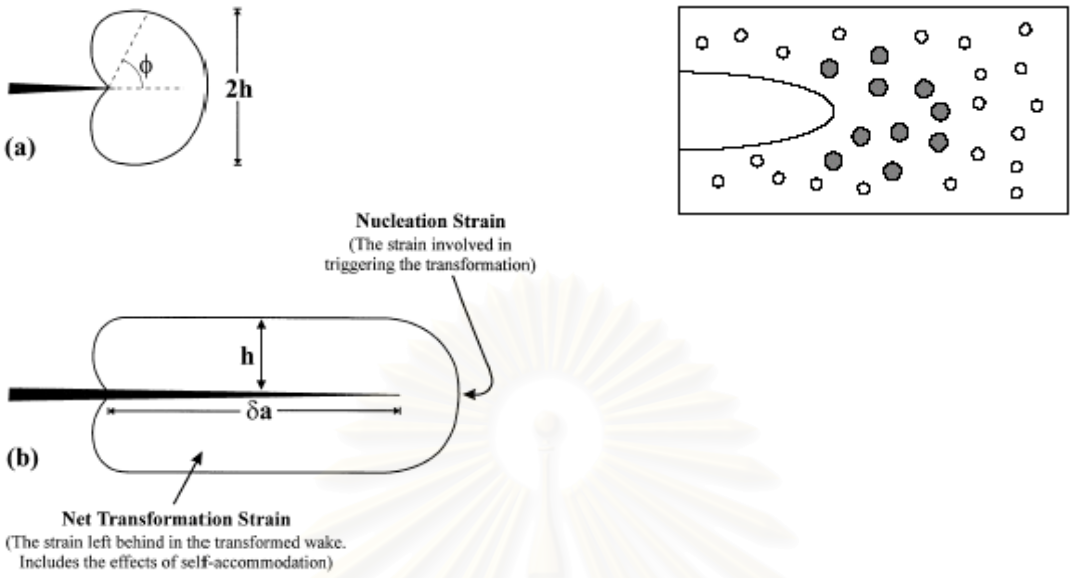

Fig.2.4 (a) Cardioids-shaped transformation zone associated with a purely dilatants transformation at a crack tip. Dotted line defines a sector at the front of the zone with an included angle of 60^{O}, which actually leads to a decrease in toughness. (b) Transformation wake of half height h associated with the movement of the crack tip by a distance δa. (c) shown the transformed phase at transformation zone

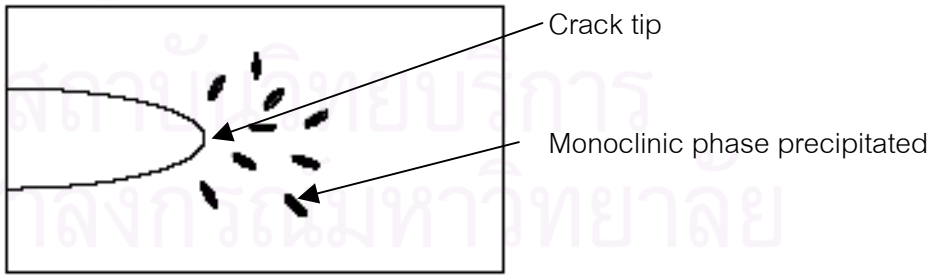

Fig.2.5 Microcrack toughening

2.2 Yttria-Tetragonal Zirconia Polycrystals

The phase diagram of Y_2O_3 - tetragonal ZrO_2 Polycrystals in the ZrO_2-rich region is shown in Fig.2.6.

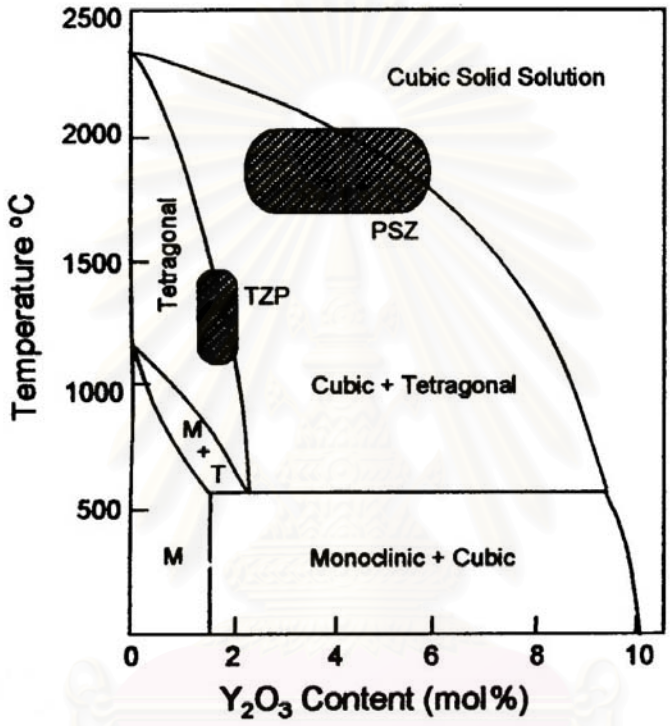

Fig.2.6 ZrO_2-rich region of the phase diagram for ZrO_2-Y_2O_3. Shaded areas indicate the compositions most commonly used for commercial engineering ceramic [11].

The content of Y_2O_3 in commercial composition of TZP is 1.75-3.50 mol% (3.5-8.7wt %). The powder is coprecipitated from zirconium nitrate solution and has size ranging from 10 to 200 nm. The powder is fired at 1300-1500^{O}C and the final grain size is ~0.5-2 μm diameter as shown in Fig.2.7. The Y_2O_3 content of PSZ is about 3-6 mol%. The tetragonal phase varies from 60% to 100%, with the remaining phase being cubic phase [11].

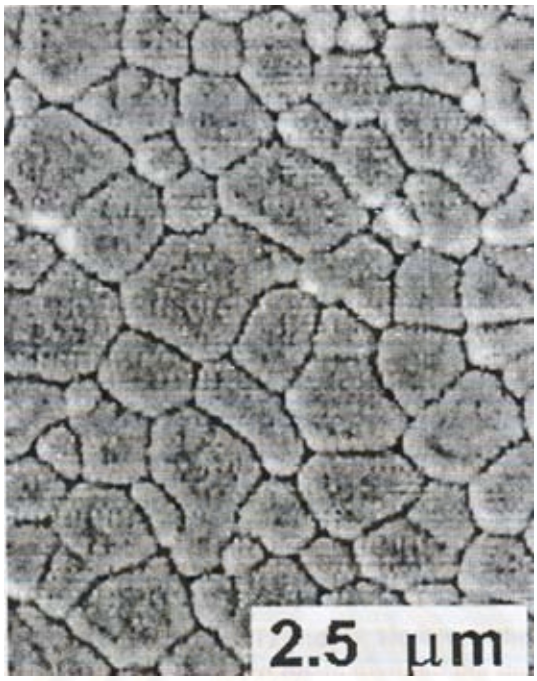

Fig.2.7 SEM microstructure of a 2.5 mol% Y-TZP material sintered 1 h at 1500^{O}C

2.3 Alumina-Zirconia Composite

Generally, various types of ceramics have high strength, but low in toughness. The addition of ZrO_2 into ceramic materials can improve this property without loosing the excellent other strength. Although, there are many factors such as type of raw materials, processing, sintering temperature, and heat treatment that concern with final properties of materials.

There are many experimental reports that studied this composite in these three decades.

N. Claussen et al. [18] observed the fracture toughness of 15 vol% ZrO_2/Al_2O_3 reached 10 MPa.$m^{1/2}$ that is twice of hot pressed Al_2O_3. The composite powder is mixed in a planetary ball mill for 60 min, and then hot pressed in graphite dies under vacuum at a pressure of 40 MPa for 30 min at 1500^{O}C. The results are illustrated in Fig.2.8.

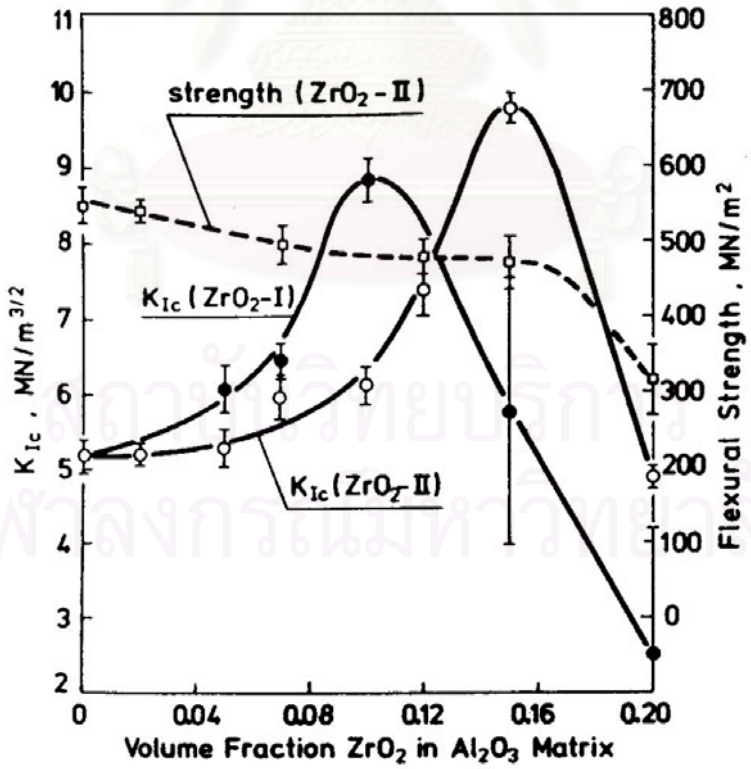

Fig.2.8 Fracture toughness and flexural strength as functions of volume fraction ZrO_2

K. Tsukuma et al. [1] measured the bending strength of ZrO_2 added 2 mol% Y_2O_3 to be 1400 MPa and its fracture toughness to be 15 MPa.$m^{1/2}$. The average bending strength increased to 2400 MPa due to the addition of 20 wt% Al_2O_3 into this ZrO_2 as a composite, and fracture toughness rose to 17 MPa.$m^{1/2}$. For the submicrometer composite powder, isostatically cold-pressed at 300 MPa and hot isostatic pressing at 1500^{O}C and 100 MPa for 30 min are used.

Yu-Seon Shin et al. [19] used hot pressed at 30 MPa, 1500^{O}C for 1 h in N_2 to fabricate 15vol% ZrO_2 /Al_2O_3 composites specimens. The highest flexural strength, 870 MPa and fracture toughness of 4.92 MPa.$m^{1/2}$ were obtained.

Furthermore, the composites composed of two types of ZrO_2 (0 mol% and 3 mol% Y_2O_3), conventionally mixed, uniaxially pressed at 44 MPa, and sintered at 1600^{O}C for 1 h were reported by W.H. Tuan et al. [13]. The strength and fracture toughness of Al_2O_3 that consisted of 10 vol% ZrO_2, 5 vol% t-ZrO_2+5 vol% m-ZrO_2, composite was 943 MPa and 7.2 MPa.$m^{1/2}$, respectively.

CHAPTER 3

EXPERIMENTAL PROCEDURES

3.1 Experimental Flowcharts

The experimental procedures are described in 3 steps, which are shown in the following flowcharts Fig. 3.1(a), (b), and (c)

Step1 Starting powder preparation

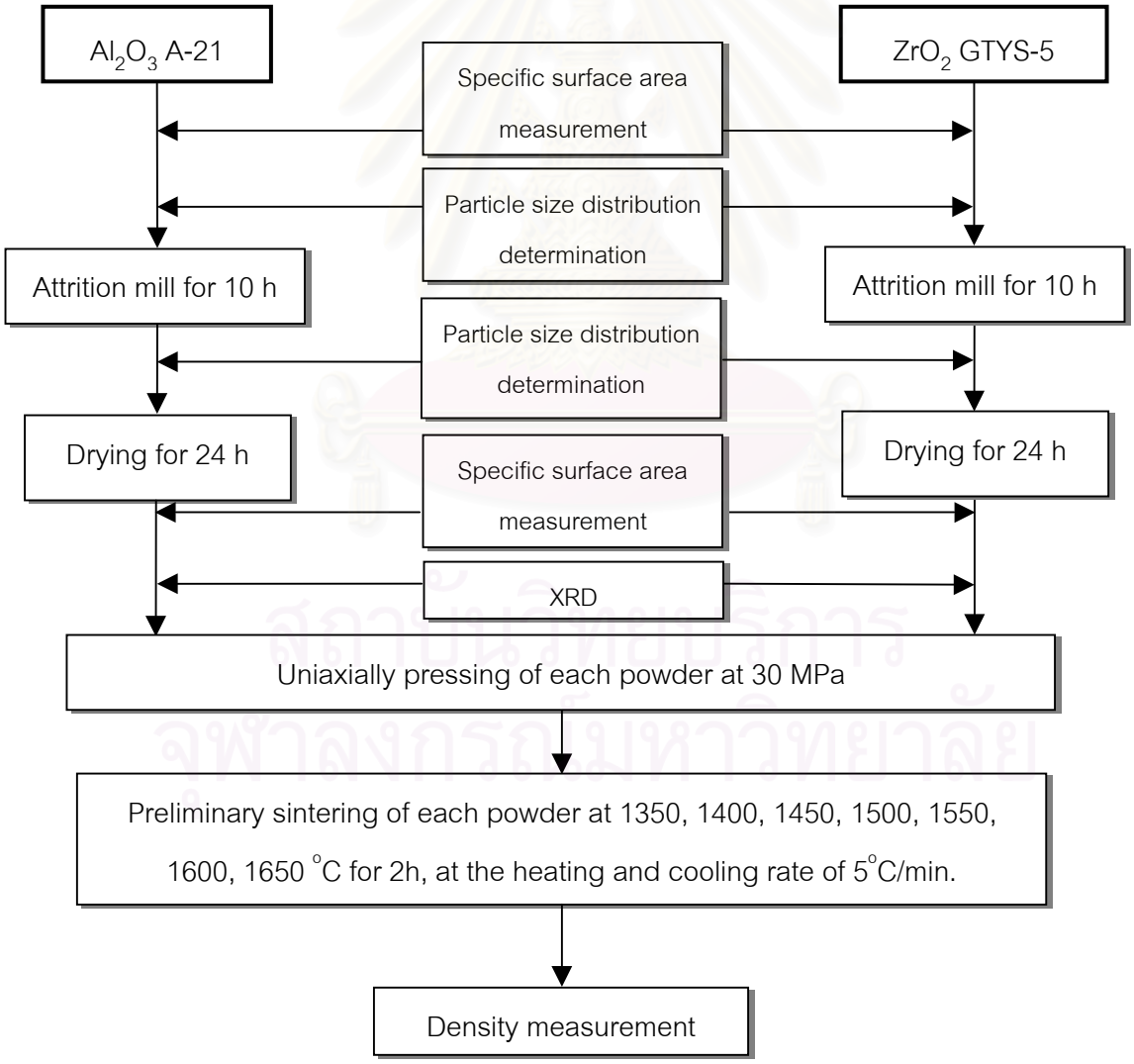

Fig 3.1 (a) Experimental flowchart, step 1 starting powder preparation

Step2 Composite preparation

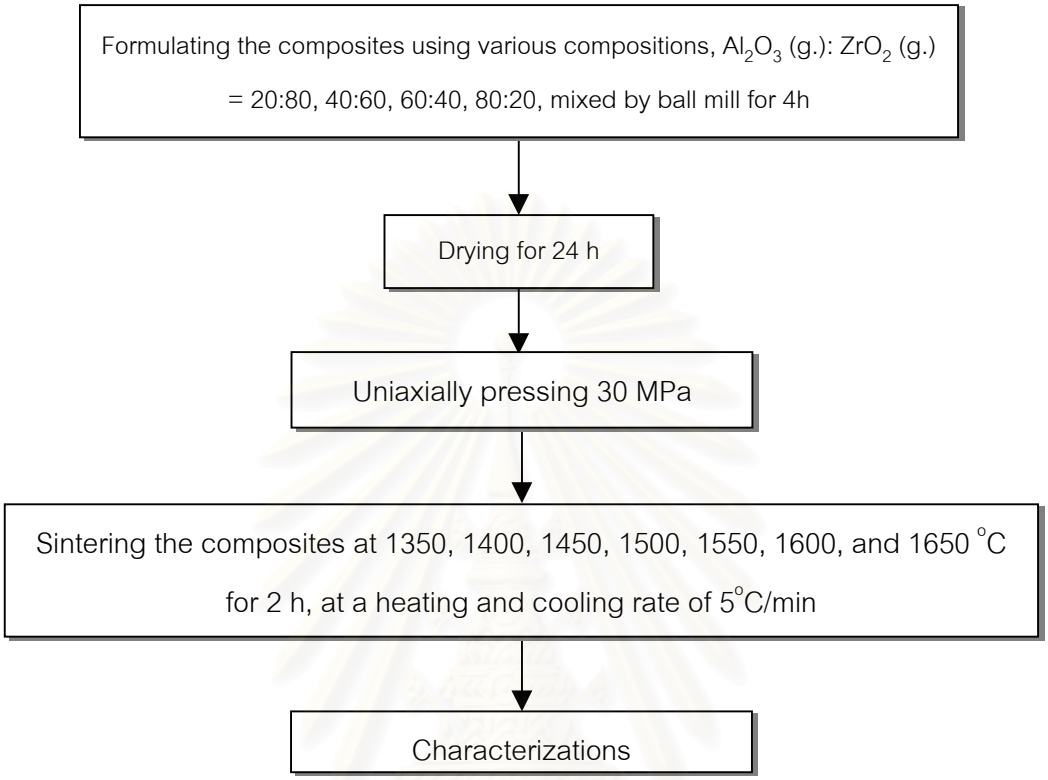

Figs 3.1 (b) Experimental flowchart, step 2 composite preparation

Step3 Characterization

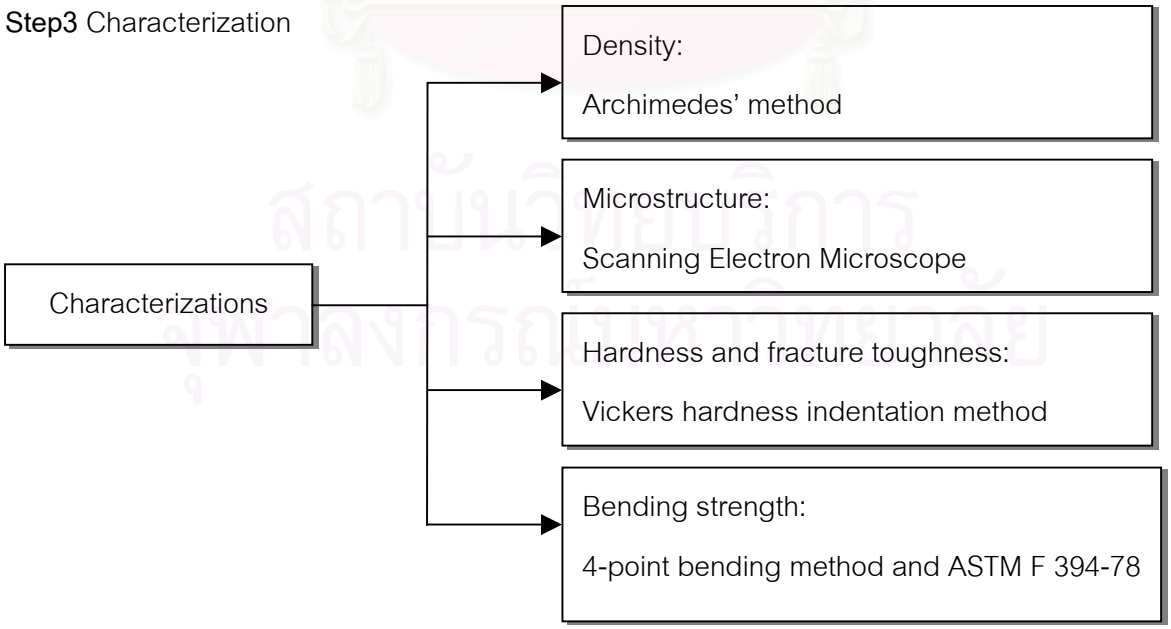

Figs 3.1 (c) Experimental flowchart, step 3 Characterization

3.2 Raw Materials and Characterizations

3.2.1 Raw Materials

The starting materials were zirconia GTYS-5 (Fukushima, Japan) and alumina A-21 (Sumitomo Chemicals, Tokyo, Japan). Typical properties received from suppliers for GTYS-5 and A-21 are shown in Table 3.1, and 3.2, respectively. The price of A-21 is about 35 baht/Kg and GTYS-5 is about 1000 baht/Kg.

Table 3.1 Typical properties of alumina, A-21

Chemical composition and properties		Qualitative data
Chemical composition (%)	H_2O	0.04
	L.O.I	0.05
	Fe_2O_3	0.01
	SiO_2	0.01
	Na_2O	0.25
	Al_2O_3	99.6
True specific gravity (g/cm^3)		3.95
Bulk density (g/cm^3)	Loosed bulk density	0.90
	Packed bulk density	1.20
Size of α-crystal (μm)		2 – 4
Linear shrinkage (%)		16
Mean particle size (μm)		50

Table 3.2 Typical properties of zirconia, GTYS-5

Chemical composition	Weight (%)
SiO_2	0.14
Fe_2O_3	0.05
TiO_2	0.21
CaO	0.08
ZrO_2 (+HfO_2)	93.71
Y_2O_3	5.61

3.2.2 Raw Materials Characterizations

3.2.2.1 Particle Size Distribution Determination

Particle size distributions of alumina A-21, and zirconia GTYS-5, were measured using dispersed sedimentation and detection by photometric method under centrifugal force with the particle size analyzer (Shimadzu SA-CP2).

About 1 gram of each raw powder was dispersed by ultrasonic dispersion in 50 cm^3 of 0.2 wt% Na-H.M.P (71600 Na-H.M.P, Flukachemic Ltd.) solution as dispersing agent for 20 min. Next, sedimentation dept No.3 and 1000 rpm of revolution were used as the condition for analysis. Then, the sample was fixed to the horizontal shaft of a motor. On one side of the disc, a rectangular sample cell was placed along the diameter of the disc. The disc was positioned so that the measuring light beam passed through the cell and a solution with 0.2 wt% Na-H.M.P was fixed on the other side of disc as a blank solution. After the motor started to rotate the disc, the measurement was made in the centrifugal sedimentation mode.

Furthermore, the particle size of raw powders and milled powders were measured using Master Sizer, S Ver.2.18, Malvern Instrument Ltd. to ensure the sizes.

3.2.2.2 Specific Surface Area measurement

The sample powders were dried in an electric furnace over night. The small amount of powders was weight and put in a specific cylinder tube for Coulter SA 3100 Surface Area and Pore Size Analyzer.

3.2.2.3 X – ray Diffraction Analysis

The sample powders of about 2-3 grams, which passed through sieve No.230 mesh (70 μm), were used for X – ray diffraction analysis (D8 ADVANCE Bruker). The condition of X - ray diffraction analysis is shown in Table 3.3.

Table 3.3 Condition of X – ray diffraction analysis

Items		Conditions
Divergence slit	(deg.)	2.0
Anti-scatter slit	(deg.)	2.0
Scan speed	(deg./min)	5.0
2θ	(deg.)	10-70
Increment	(deg.)	0.1
Step time	(sec.)	2.4
Current	(mA)	30
Voltage	(kV)	40

3.3 Preliminary Sintering of Alumina and Zirconia

Each powder was prepared for preliminary sintering as shown in Fig.3.1 (a). The raw material was milled in an attrition mill for 10 h using the condition shown in Table 3.4. The diameters of alumina media balls were 3 mm, and 5 mm and zirconia media balls were 5 mm in diameter. The media balls were filled to a half volume of the zirconia mill (1100 cm^3) with 220 grams of raw powders and 200 cm^3 of distilled water as medium. After 10 h, the milled powders were dried at 100°C overnight in an oven to evaporate water.

The milled powders were mixed with 1.0 wt% of polyvinyl alcohol (PVA 10000 – 15000 MW, 13 grams of polyvinyl alcohol to 87 grams of water) as binder and sieved through a 100-mesh screen. Then, 3.5 grams of these powders were pressed into pellets of 25 mm in diameter by uniaxial press at the pressure of 30 MPa. All specimens were dried overnight at 100°C in an oven for humidity removal. Further, the specimens were heated at 300°C for 1 h with a heating rated 5°C/min to remove binder and the temperature was elevated with the same heating rate to 1350, 1400, 1450, 1500, 1550, 1600, and 1650°C and was kept for 2 h. Finally, the specimens were cooled down to 35°C at the similar heating rate.

Table 3.4 Condition of attrition mill

Condition	Alumina A-21	Zirconia GTYS-5	Zirconia GTYS-5
Weight of powder (g.)	220	200	200
Type of media balls	Al_2O_3	Al_2O_3	ZrO_2
Diameter of media balls (mm.)	3	3	5
Weight of media balls (g.)	1215	1215	1615
Weight of water (g.)	180	200	200
Rotor speed (rpm)	550	550	550
Time of milling (h.)	10	10	10

3.4 Composition and Preparation of Alumina-Zirconia composite powder

The compositions of the composite were varied from 100 wt% Al_2O_3 - ZrO_2 to Al_2O_3 – 100 wt% ZrO_2 as shown in Table 3.5.

Table 3.5 Compositions of the composite

Specimen	100A0Z	80A20Z	60A40Z	40A60Z	20A80Z	0A100Z
Al_2O_3 milled powder (wt %)	100	80	60	40	20	0
ZrO_2 milled powder (wt %)	0	20	40	60	80	100

The preparation of composite is illustrated in the flowchart, Fig.3.1 (b), and it was prepared by ball mill mixed process. As the starting powders, both milled powders of alumina and zirconia were used. The milled powders were mixed in a polypropylene bottle (250 cm^3) for 4 hours, using alumina balls as grinding media filled to a half of the bottle with 100 cm^3 of distilled water as medium. Next, the mixture was filtered and dried at 100°C overnight in an oven to remove water. Then, the mixed composite powders were processed at the same conditions written in 3.3. Then, it was uniaxially pressed at a pressure of 30 MPa using 3, 3.5 and 9 grams of powders into pellets of 20, 25 and 38 mm in diameter. All specimens were dried overnight at 100°C in an oven for humidity removal. Further, the specimens were sintered at the same conditions written in 3.3.

3.5 Characterization of Sintered Specimens

3.5.1 Density measurement

3.5.1.1 Bulk density

The Archimedes' method was used to measure the bulk density. The specimens were placed in a vacuum chamber to remove the air in open pores for 30 min. Water was poured onto specimens until all specimens were submerged in water while the chamber was in a vacuum and was kept for 30 min. The density of the sample was calculated using equation (3.1) following ASTM standard (designation: C830-93)

$$\text{Bulk density} = \frac{W_d}{W_{sus} - W_{sat}} \bullet \rho_{water} \quad (3.1)$$

Where W_d is dry weight

W_{sat} is water-saturated weight

W_{sus} is suspended weight in water

3.5.1.2 Theoretical density

The theoretical density of sintered body of composite was estimated from the rule of mixture as shown in equation (3.2)

$$\text{Theoretical density} = \frac{W_{total}}{\frac{W_1}{\rho_1} + \frac{W_2}{\rho_2} + ...} \quad (3.2)$$

Where W_{total} is total weight of used components.

W_1, W_2 is weight of 1st and 2nd component, respectively.

ρ_1, ρ_2 is real density of 1st and 2nd component, respectively.

1, 2,…. is number of used component.

In this experiment, the theoretical densities of pure Al_2O_3 A-21 and ZrO_2 GTYS-5, 3.95 g/cm^3 and 6.05 g/cm^3 [2] were used for the calculation, respectively. As a result the theoretical densities of composites are shown in Table 3.6

Table 3.6 Theoretical density of each composite

Composite	Calculated theoretical density (g/cm^3)
100A0Z	3.95
80A20Z	4.24
60A40Z	4.58
40A60Z	4.97
20A80Z	5.44
0A100Z	6.05

3.5.1.3 Percent of theoretical density

The relative density was calculated from bulk density and theoretical density using equation (3.3).

$$\% \text{ of theoretical density} = \frac{\text{Bulk density}}{\text{Theoretical density}} \bullet 100 \qquad (3.3)$$

3.5.1.4 Water absorption measurement

The Archimedes' method was used to calculate the water absorption of sintered specimens as shown in equation (3.4).

$$\% \text{ of Water absorption} = \frac{W_{sat} - W_d}{W_d} \bullet 100 \qquad (3.4)$$

Where W_d is dry weight

W_{sat} is water saturated weight

3.5.2 Microstructure Examination by Scanning Electron Microscope (SEM)

The microstructures of sintered specimens were examined by a scanning electron microscope (SEM) (JEOL: JSM-1670). The specimens were polished with several numbers of silicon carbide papers using Buehler machine (PHOENIX 4000, Buehler Co. Ltd.) with 20 pound loading and 200 rpm at each size. Finally, specimens were finished with diamond paste of 1 μm for 15 min. Then, all specimens were thermally etched at 1500°C for 1 hour. After that, they were gold sputtered before put into the microscope. The process mentioned is schematically shown in Fig.3.2.

Grain size was determined by counting followed by calculation the number of equivalent diameter size of each particle.

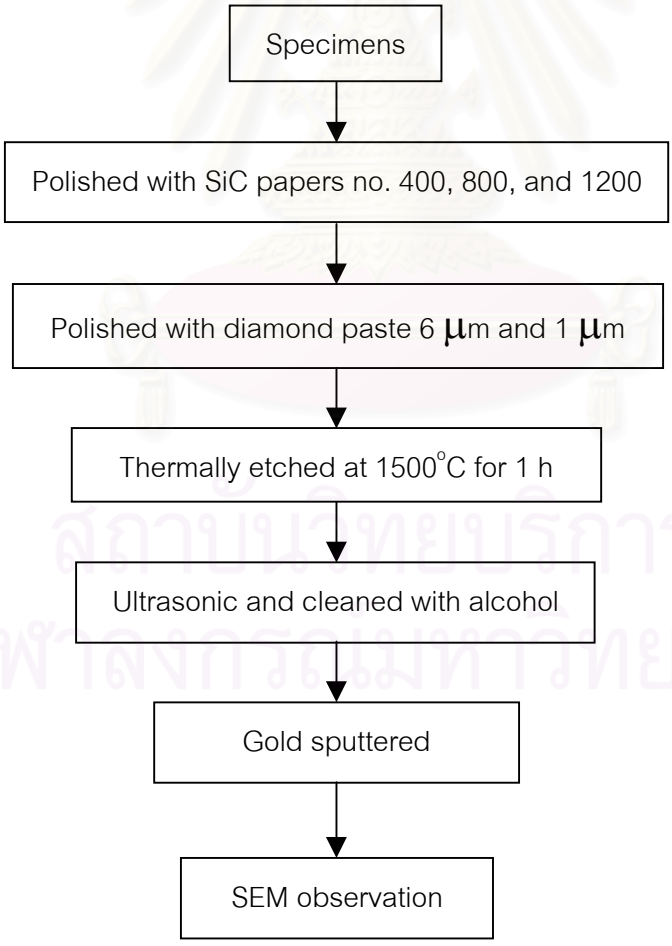

Fig.3.2 Flowchart of sample preparation for SEM observation

3.5.3 Vickers Hardness and Fracture Toughness Measurement

The Vickers indentation method with 10 Kg loading (98.07 N), Zwick 3212, Zwick GmbH & Co. was used to measure hardness and fracture toughness.

The surface of specimen was polished under the same conditions written in 3.5.2.

Vickers hardness (H_V) was calculated according to JIS (R1610-1991) through the following equation:

$$H_V = 1.8544 \times \left[\frac{P}{(2a)^2} \right] \quad (3.5)$$

Where P is load (N)

a is length of diagonal (m)

Fracture toughness (K_{1C}) was calculated according to JIS (R1607-1995) through the following equation:

$$K_{1C} = 0.0026 \times \left[\frac{E^{1/2} P^{1/2} a}{c^{3/2}} \right] \quad (3.6)$$

Where E is elastic modulus (Pa)

c is crack length (m)

In this experiment, the elastic moduli of alumina and zirconia, 390 GPa and 190 GPa [6] were used, respectively.

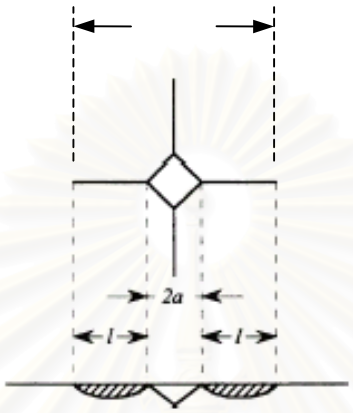

Fig.3.3 Configuration of the cracks for the Vickers hardness indentation [3]

3.5.4 Strength Measurement

The sintered specimen (38 mm diameter) was ground with no.400 and 800 diamond wheels and then polished with 2000 mesh silicon carbide powder for 1 hour, 8000 mesh for 30 min, 3 μm of diamond paste for 15 min and finally polished with 1 μm of diamond paste for 10 min.

The compression side of each specimen was attached by a piece of Scotch tape to prevent the scatter of specimen after breaking. Then the specimen was placed on three symmetrically spaced points near its perimeter, next the force was applied to the center of specimen with constant cross head speed of 0.5 mm/min (LLOYD 500, Intro Enterprise Co. Ltd.)

The load of breaking dimensions of specimen, radii of support and loaded area were used to calculate the maximum tensile stress by the equation (3.7) in conformity with the ASTM standard (F 394-78).

$$S = -0.2387\,P\,\frac{(x - y)}{d^2} \qquad (3.7)$$

Where

S	=	maximum center tensile stress (MPa)
P	=	total load causing fracture (N)
x	=	$(1+\upsilon)\ln\left(\frac{B}{C}\right)^2 + \left[\left(\frac{1-\upsilon}{2}\right)\right]\left(\frac{B}{C}\right)^2$
y	=	$(1+\upsilon)\left[1+\ln\left(\frac{A}{C}\right)^2\right] + (1-\upsilon)\left(\frac{A}{C}\right)^2$
υ	=	Poisson's ratio, 0.23
A	=	radius of support circle (mm), 12.5 mm
B	=	radius of loaded area or ram tip (mm), 1.5 mm
C	=	radius of specimen (mm)
d	=	specimen thickness at fracture origin (mm)

CHAPTER 4

EXPERIMENTAL RESULTS AND DISCUSSIONS

4.1 Raw Materials Characterization

4.1.1 Particle size distribution

Each raw material was milled by attrition mill for 10 h (Appendix 1) and sampled at 15, 30 min, 1, 2, 3, 5, 7, and 10 h, respectively.

The average particle sizes of Al_2O_3 A-21 before and after milling are shown in Fig.4.1 (a), and (b). The average particle size of ZrO_2 GTYS-5 after milling is only a little smaller than that of raw material, but large particles included in raw powder were comminuted as shown in Fig.4.1 (c), and (d). The average particle size at 50 % cumulative of Al_2O_3 A-21 milled for 10 h with Al_2O_3 balls is 0.73 μm and those of ZrO_2 GTYS-5 milled for 10 h with Al_2O_3 balls and ZrO_2 balls are 0.44 and 0.57 μm, respectively. So, the difference of average particle size between milled A-21 and milled GTYS-5 is not much and shown in Table. 4.1. The particle size distribution curves show the same tendency as shown in Appendix 2.

The particle sizes of raw powders measured are smaller than the value in the specification of suppliers. It is supposed that the values from suppliers indicate the agglomerated particle size.

Table 4.1 Average particle size of powders after milling

Type of powder	Milling condition	Time of milling (min)	Average particle size (μm)
Al_2O_3 A-21	Al_2O_3 balls	15	4.45
		30	3.9
		60	3.7
		120	1.7
		180	1.3
		300	1.1
		420	0.75
		600	0.73
ZrO_2 GTYS-5	Al_2O_3 balls	15	0.63
		30	0.57
		60	0.48
		120	0.48
		180	0.50
		300	0.51
		420	0.47
		600	0.44
ZrO_2 GTYS-5	ZrO_2 balls	15	0.76
		30	0.64
		60	0.63
		120	0.63
		180	0.62
		300	0.61
		420	0.60
		600	0.57

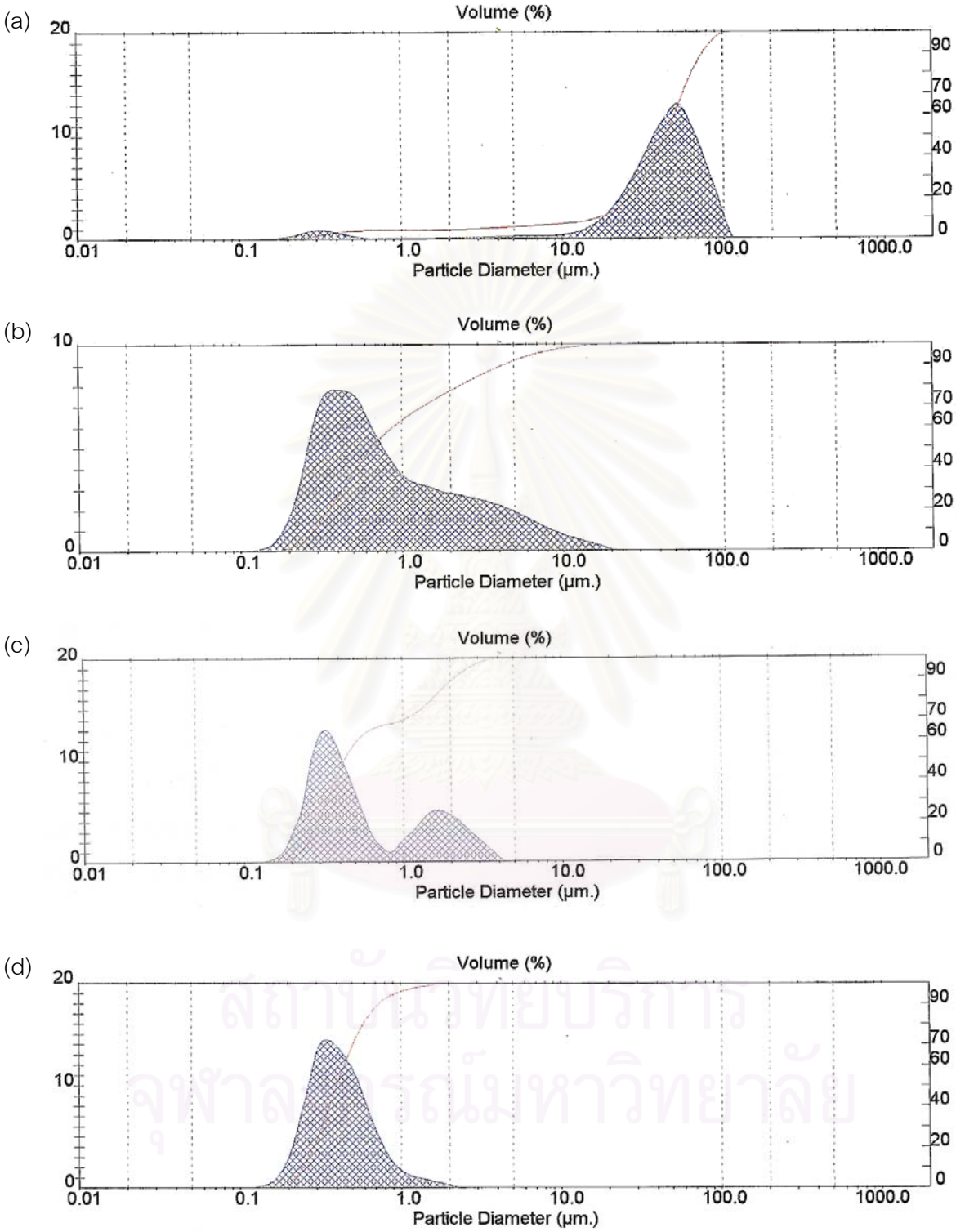

Fig.4.1 Particle size distribution of raw powders and milled powders (a) Al_2O_3 A-21, (b) Al_2O_3 A-21 milled 10h with Al_2O_3 balls, (c) ZrO_2 GTYS-5, and (d) ZrO_2 GTYS-5 milled 10h with ZrO_2 balls

4.1.2 Surface area measurement

The specific surface areas (SSA) of raw powders and milled powders are measured by BET method. The results are shown in Table 4.2.

After milling in the attrition mill for 10 h the SSA of A-21 increases dramatically from 0.66 to 18.6 m^2/g. The specific surface area of GTYS-5 milled for 10 h is higher than raw powder, too. It increases from 6.1 to 8.3 m^2/g. The tendency of increment of SSA corresponds to the particle size distribution change.

Table 4.2 Specific surface areas of powders

powder		Specific surface area (m^2/g)
A-21	as-received	0.66
	milled 10 h with Al_2O_3 balls	18.6
GTYS-5	as-received	6.1
	milled 10 h with ZrO_2 balls	8.3

4.1.2 X-ray diffraction (XRD) analysis

The X-ray diffraction analyses of raw powders and milled powders are shown in Fig.4.2 (a) XRD pattern of Al_2O_3 A-21 (b) XRD pattern of Y_2O_3 partially stabilized ZrO_2 [20]. The patterns of the milled powder are the same as the raw powders. It indicates that the phase of powder did not change by milling under the experimental condition. The broader and lower intensity of milled powders compared to the as received might result from the much finer particle size (submicrometer) obtained from the attrition mill.

(a) Alumina (A-21)

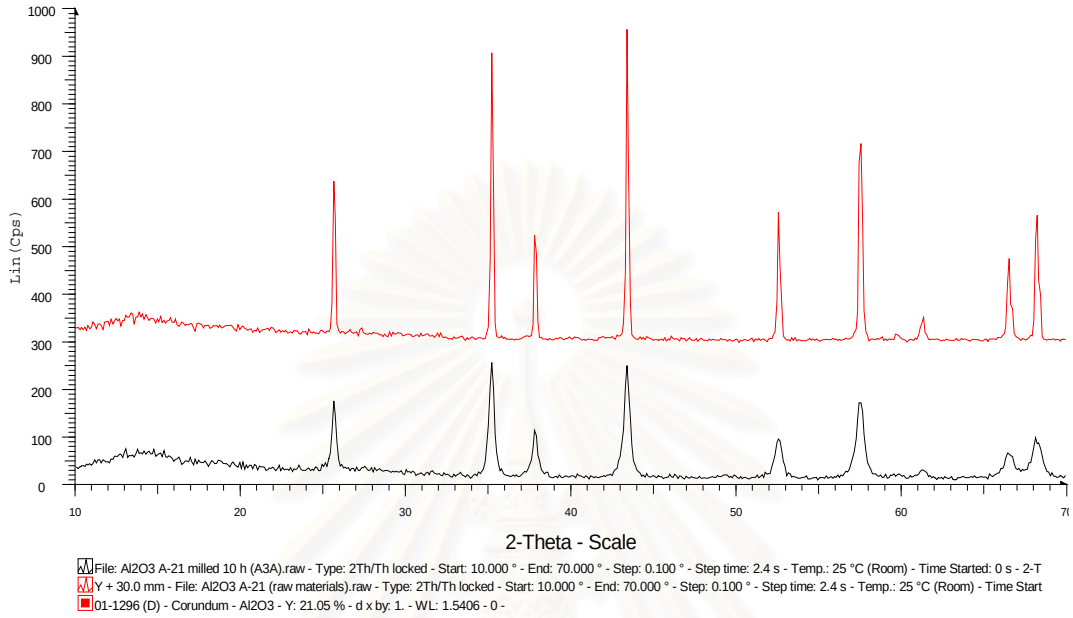

(b) Zirconia (GTYS-5)

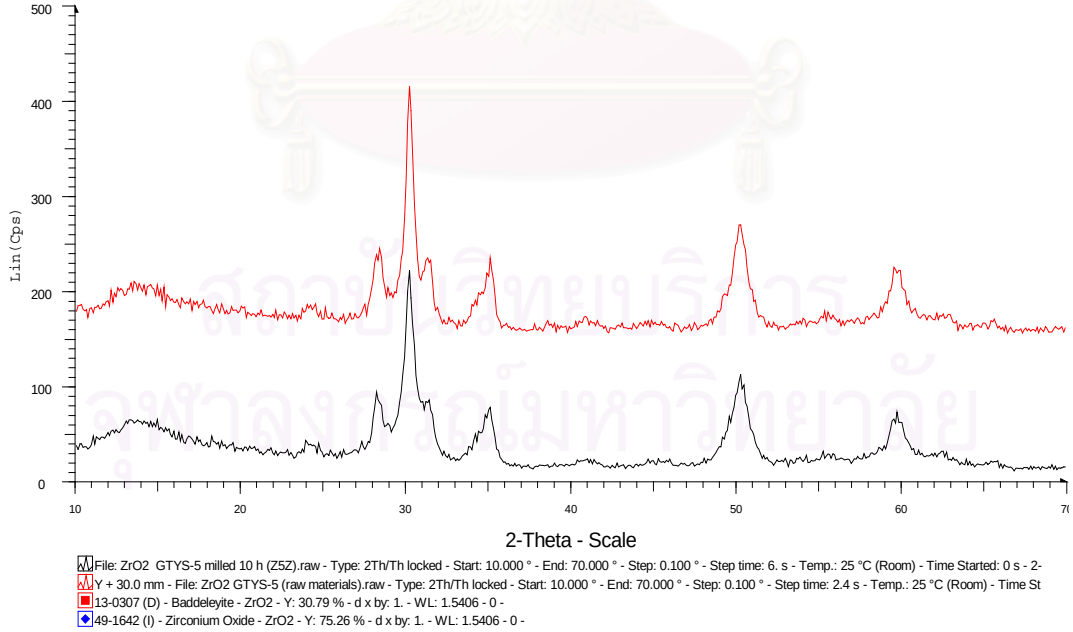

Fig.4.2 X-ray diffraction patterns of (a) Al_2O_3 A-21 and (b) ZrO_2 GTYS-5. The red line is raw powder from supplier and black line is milled powder for 10 h.

4.2 Preliminary Sintering of Alumina and Zirconia

The pressed pellets were sintered at various temperatures, 1350, 1400, 1450, 1500, 1550, 1600, and 1650^{O}C for 2 h. The relationship between relative density and sintering temperature is shown in Fig.4.3. The relationship between relative density and sintering temperature of all specimens are shown in Appendix 3.

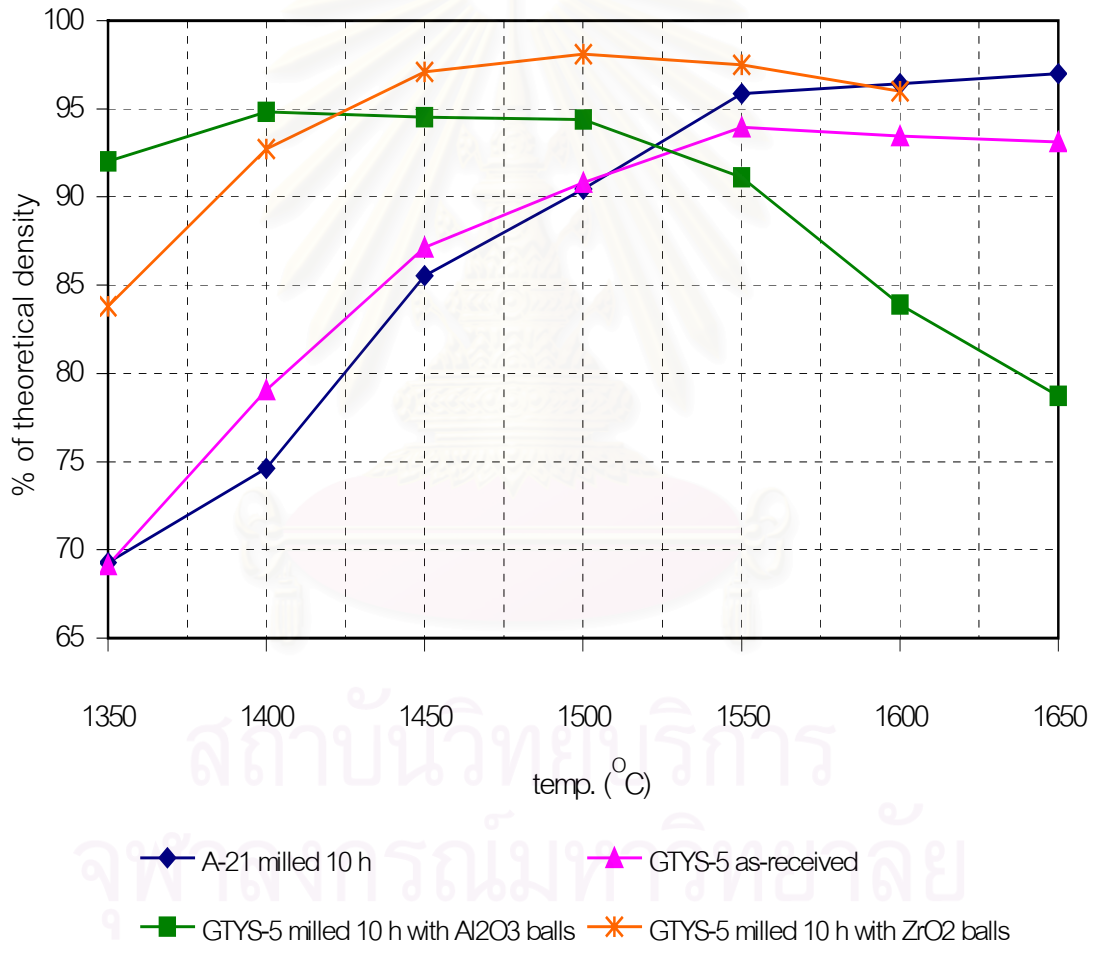

Fig.4.3 Relationship between% of theoretical density and sintering temperature of each powder

Al_2O_3 milled for 10 h consolidates to almost full density at 1550^{O}C and the density increases with elevating temperature. As-received ZrO_2 also consolidates to high density at 1550^{O}C; however, the value is lower than 94%. ZrO_2 milled for 10 h with Al_2O_3 balls consolidates at low temperature as 1400^{O}C to 94%. However, the relative density decreases at temperature over 1550^{O}C. ZrO_2 milled for 10 h with ZrO_2 balls does not consolidate to such low density, however, the density becomes so high as 96-98% of theoretical density at 1450-1600^{O}C.

The average particle sizes of ZrO_2, as-received and milled for 10 h are not so different, however, the particle size distribution curves are very different as shown in Fig.4.1(c), and (d). The particle size distribution of the as-received ZrO_2 is bimodal. Those large particles over 1.0 μm may inhibit the densification of the as-received ZrO_2 at low temperature region.

The microstructures of ZrO_2 milled for 10 h with Al_2O_3 balls, pressed into pellets and sintered at 1500 and 1650^{O}C are shown in Fig.4.4. (a) and (b). The back scattering SEM micrographs show the bright part is ZrO_2 grain and black part is Al_2O_3 grains as a contaminant from milling process. Al_2O_3 enhances the densification of ZrO_2 at 1350-1500^{O}C [21]. It shows the relative density higher than the as-received ZrO_2 as shown in Fig.4.3. The reduction in sintered density of specimens at temperature over 1500^{O}C accompanies with the increase in grain size as shown in Fig.4.4 (b).

(a)

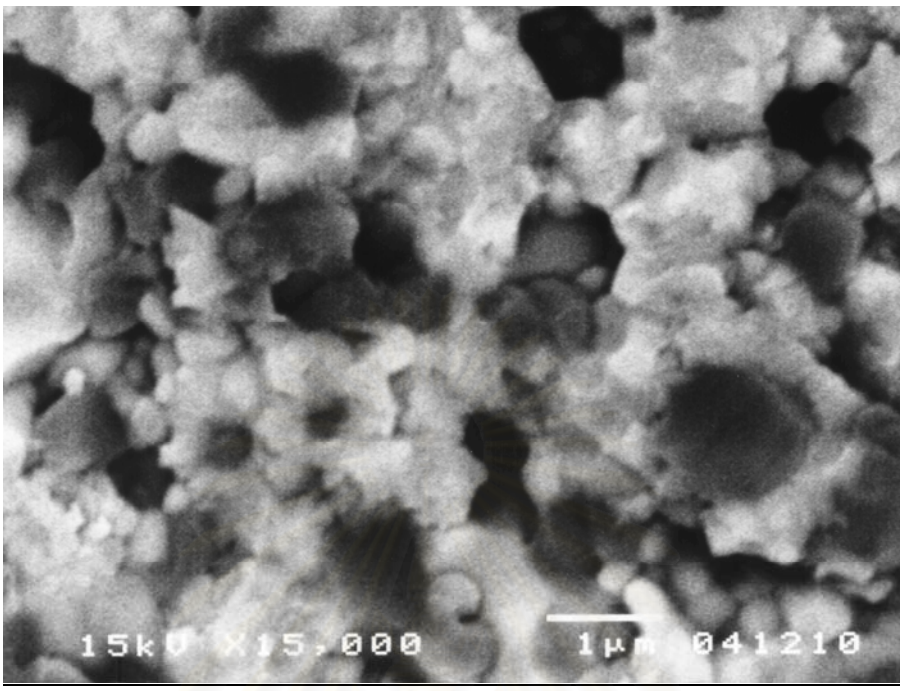

(b)

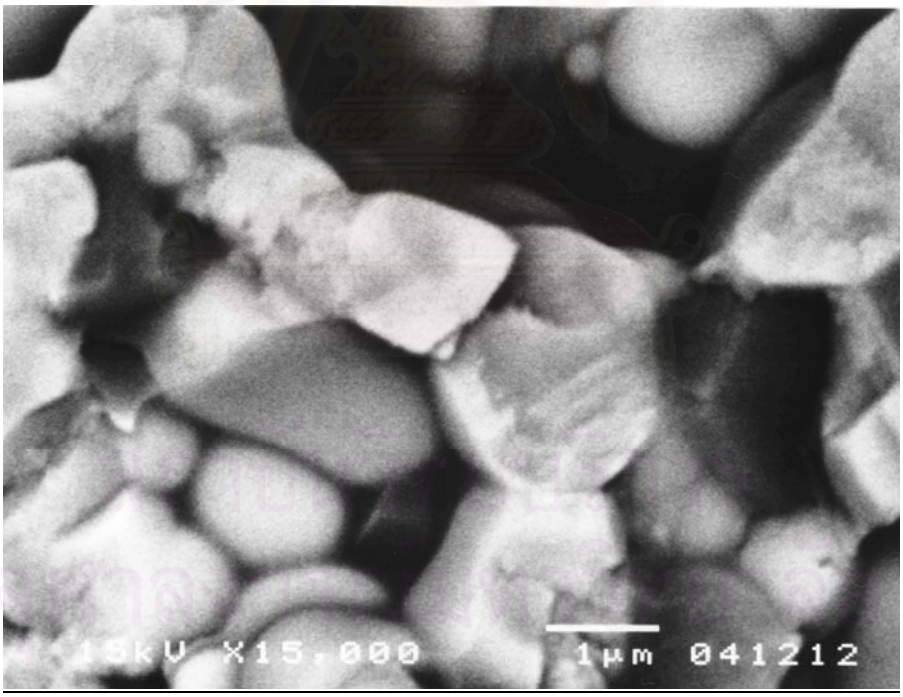

Fig.4.4 Fractured surface of ZrO_2 specimen (a) and (b) Black scattering SEM micrograph of milled ZrO_2 specimen sintered at 1500, and 1650^{O}C, respectively

4.3 Characterization of Sintered Alumina - Zirconia Composite Specimens

The milled A-21 and milled GTYS-5 with ZrO_2 balls were mixed into 6 composite compositions as shown in Table 3.5. They were designated as 100Z, 80Z20A, 60Z40A, 40Z60A, 20Z80A, and 100A. The number was referred to weight percent of compositions, the capital letters A, and Z was referred to Al_2O_3, and ZrO_2 components, respectively. They were sintered at the same condition with the preliminary sintering of raw powders. The relationship of density and sintering temperature of composites is shown in Fig.4.5, and the relationships of all samples are shown in Appendix 4.

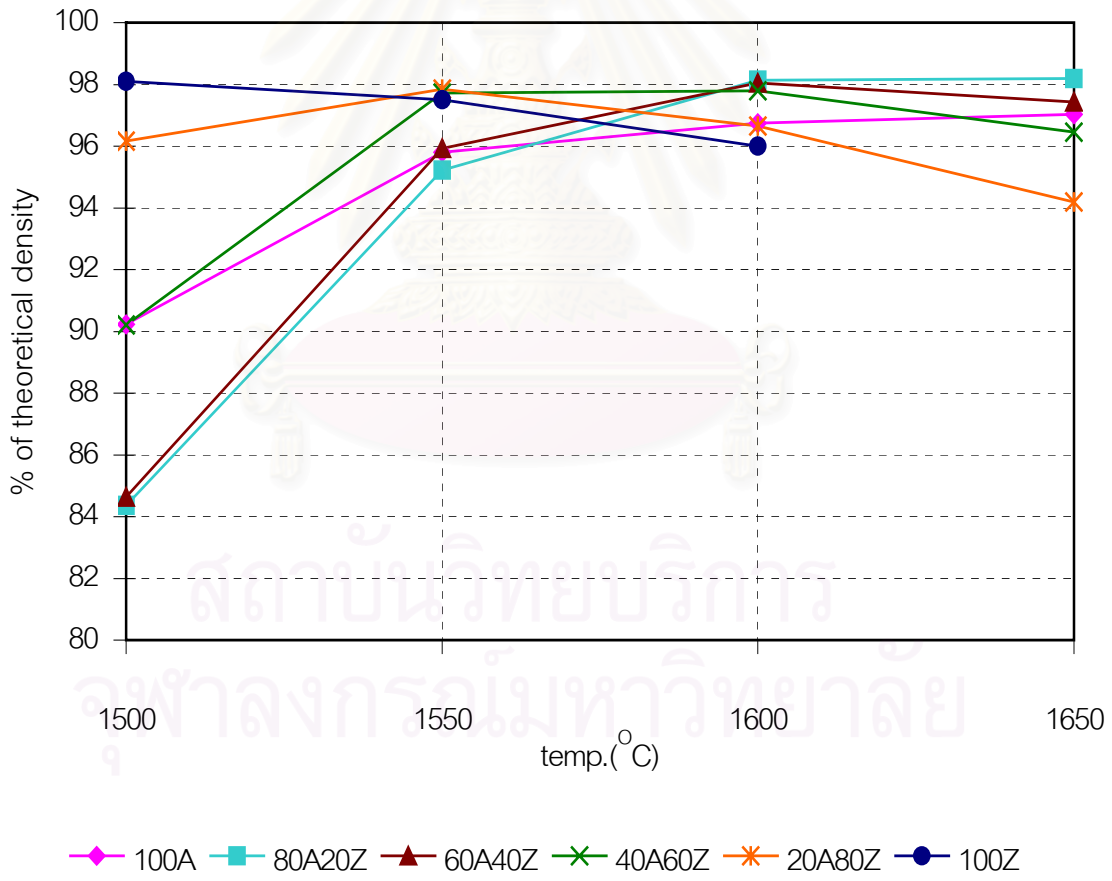

Fig.4.5 Relationship of % of theoretical density and sintering temperature of composites

The theoretical densities shown in Table 3.6 were used to calculate the relative density of the composites and expressed in terms of % of theoretical density. Density of composite almost reached to theoretical density at temperatures of 1550-1600^{O}C. They can be classified into two groups at 1550^{O}C. Group 1 includes higher weight percent of GTYS-5, i.e. pure GTYS-5, 80%, and 60%. Group 2 includes higher weight percent of A-21, i.e. pure A-21, 80%, and 60%. Group 1 shows the higher densities at lower temperature than Group 2, but they decrease when sintering temperature rises over 1550^{O}C. On the other hand, the densities of Group 2 increase with increasing sintering temperature. This tendency is similar to the densities of the major (the higher content) components of composites.

4.4 Microstructure observation of Composite by SEM

SEM micrographs of the composites are illustrated in Fig. 4.6. The bright grain is ZrO_2 and dark grain is Al_2O_3 and grain shapes remain equiaxed. The average grain sizes of the composites are shown in Fig. 4.7, and the data are attached in Appendix 5.

(a)

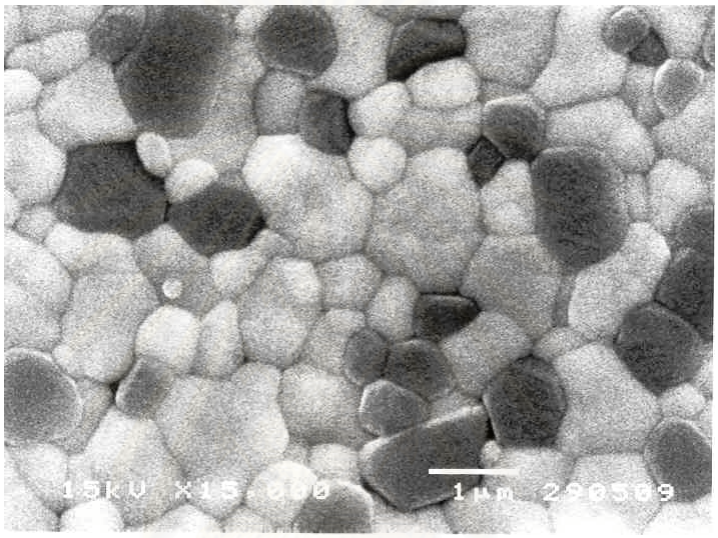

(b)

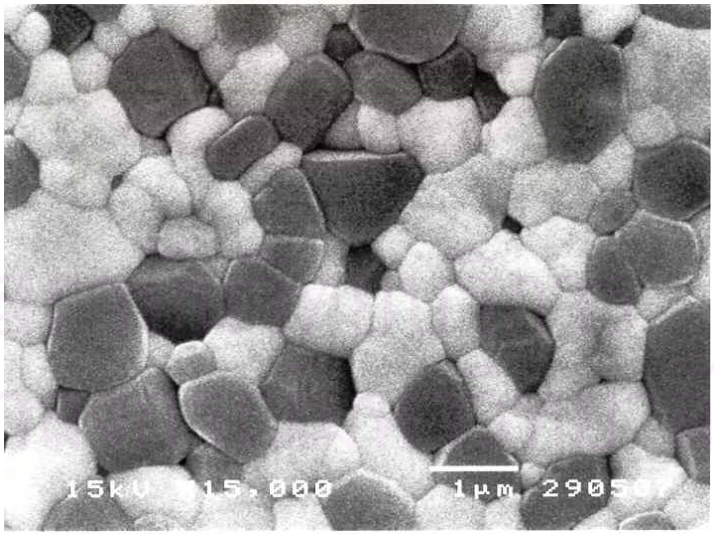

Fig.4.6 SEM micrographs of Al_2O_3-ZrO_2 composites sintered at 1600^{O}C for 2 h (a) 20A80Z, and (b) 40A60Z.

(c)

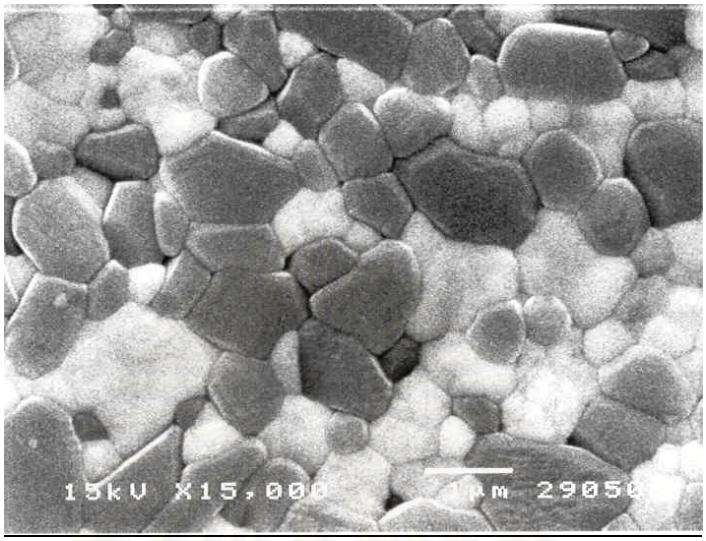

(d)

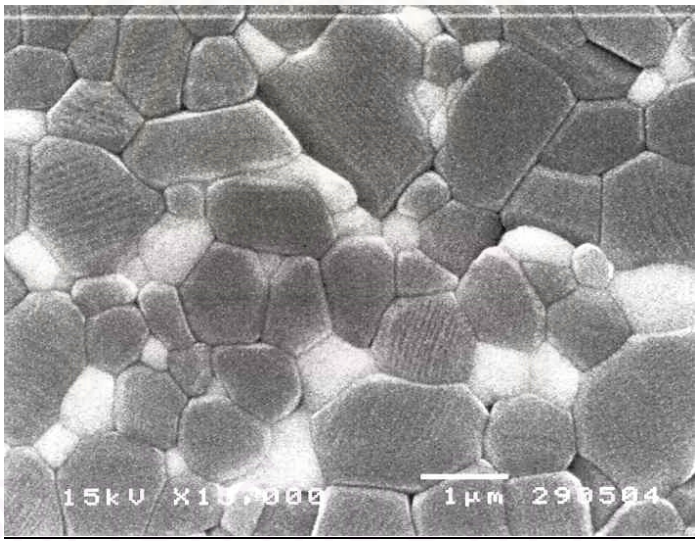

Fig.4.6 SEM micrographs of Al_2O_3-ZrO_2 composites sintered at 1600^{O}C for 2 h (c) 60A40Z, and (d) 80A20Z.

The Al_2O_3 and ZrO_2 phases are almost well dispersed except at high content where there is some apparent clustering of the phases [22]. All of the composites exhibit nearly full density (≥96% as shown in Appendix 5), and fine grain size. Grain size distributions of all specimens are attached in Appendix 6, and the average grain size of Al_2O_3 compared with ZrO_2 is shown in Fig.4.7. The average grain size of Al_2O_3 decreases when ZrO_2 content increases, the ZrO_2 grains predominantly beside at the grain boundary of Al_2O_3 effectively pin the Al_2O_3 grain boundary and limit the Al_2O_3 grain size. The average grain size of Al_2O_3 ranges from 2.5 to 0.9 μm. The average grain size of ZrO_2 varies from 0.8 to 2.4 μm. The smallest size of ZrO_2 grain occurred at the largest Al_2O_3 content.

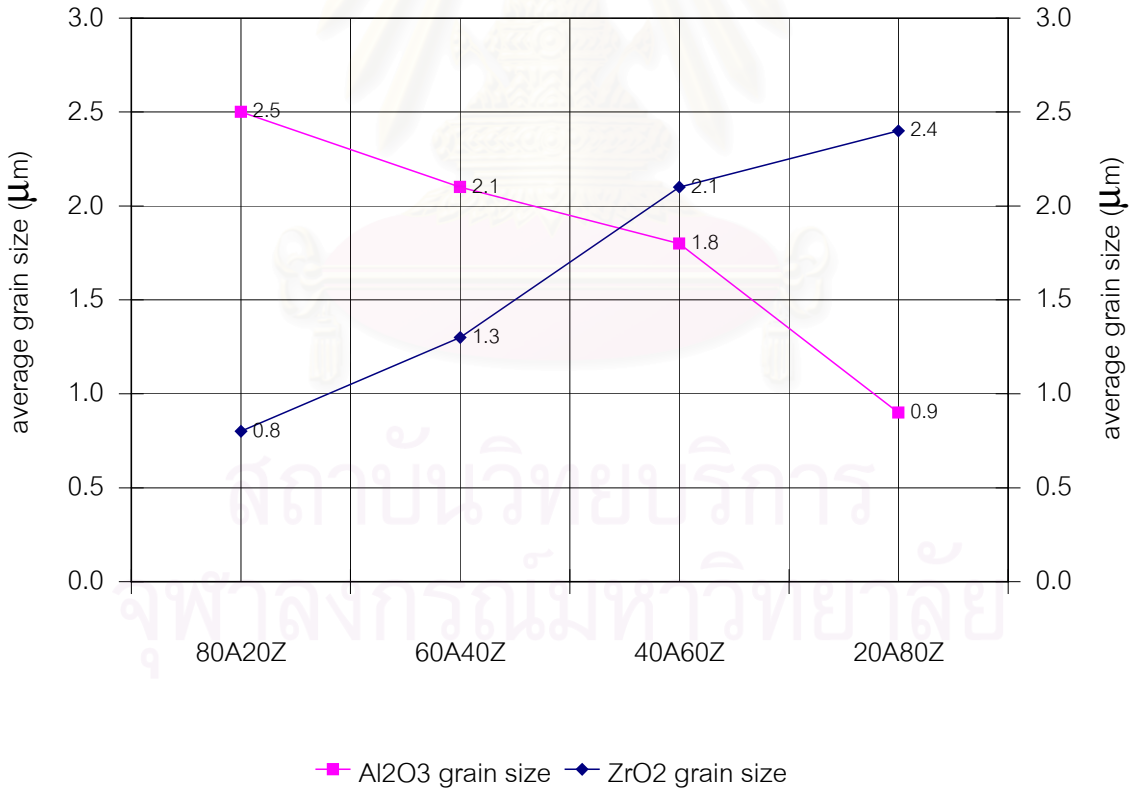

Fig.4.7 Average grain size of alumina-zirconia composite sintered at 1600°C for 2 h

4.5 Vickers Hardness and Fracture Toughness Measurement

The trends of Vickers hardness (H_v) and fracture toughness (K_{1c}) as a function of Al_2O_3 content are shown in Fig.4.8. The H_v and K_{1c} were calculated from equation 3.5, and equation 3.6, respectively. The details of all data are shown in Appendix 7. Starting from the pure ZrO_2, H_v increases with the increase in Al_2O_3 content, and the maximum value for 80A20Z is 15.95 GPa. K_{1c} increases with the increase in Al_2O_3 content, and the maximum value for 20A80Z and 80A20Z is 6.0 MPa.$m^{1/2}$, and decreases dramatically for 60A40Z (5.3 MPa.$m^{1/2}$). The composites 40A60Z and 60A40Z are distinguished by close size of the Al_2O_3 and ZrO_2 grains (size ratio is 1.17 and 1.62) as shown in Appendix 6.

Generally, the increase of tetragonal ZrO_2 involves the increase of K_{1c} due to the phase transformation of ZrO_2. Fig.4.9 shows the tendency of K_{1c} is similar to the tendency of grain size ratio as shown in Appendix 5. Therefore, the increase of the fracture toughness is related to the presence of the large difference in two grains, in other word, inhomogeneous morphology might be the cause of large K_{1c}.

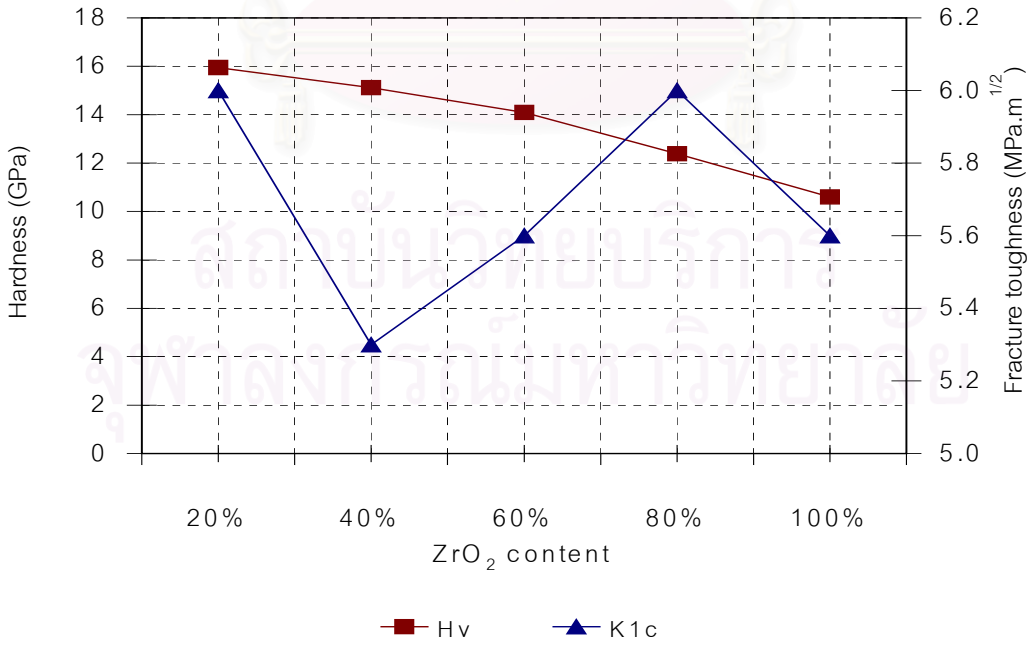

Fig.4.8 Vickers hardness and Fracture toughness as a function of ZrO_2 content of Al_2O_3-ZrO_2 composite sintered at 1600^{O}C for 2 h.

Annamaria Celli et al. [23] reported the sketch of crack paths of Al_2O_3-ZrO_2 composite that appeared at the corner of indentation as referred in Appendix 8. The crack shape depended on the material composition and related with the average grain size of Al_2O_3 grains. The average grain size of Al_2O_3 increased with increasing Al_2O_3 content. There was a decrease in average grain size of Al_2O_3 from the sample with a high percentage of Al_2O_3, 80A20Z to 60A40Z. Therefore, it is possible to assume that the crack tends to follow the Al_2O_3 grain boundaries and the bend of crack path decreases as the Al_2O_3 grain size decreases. Besides the t→m transformation, it is suggested that transgranular fracture is the main fracture mechanism in the specimens with high zirconia content, 100Z and 20A80Z, as shown if Fig.4.9 and as referred to Appendix 8. The change of the bend of crack path between 100Z and 20A80Z can not be investigated. Thus microstructure and composition do not affect the toughness of these materials.

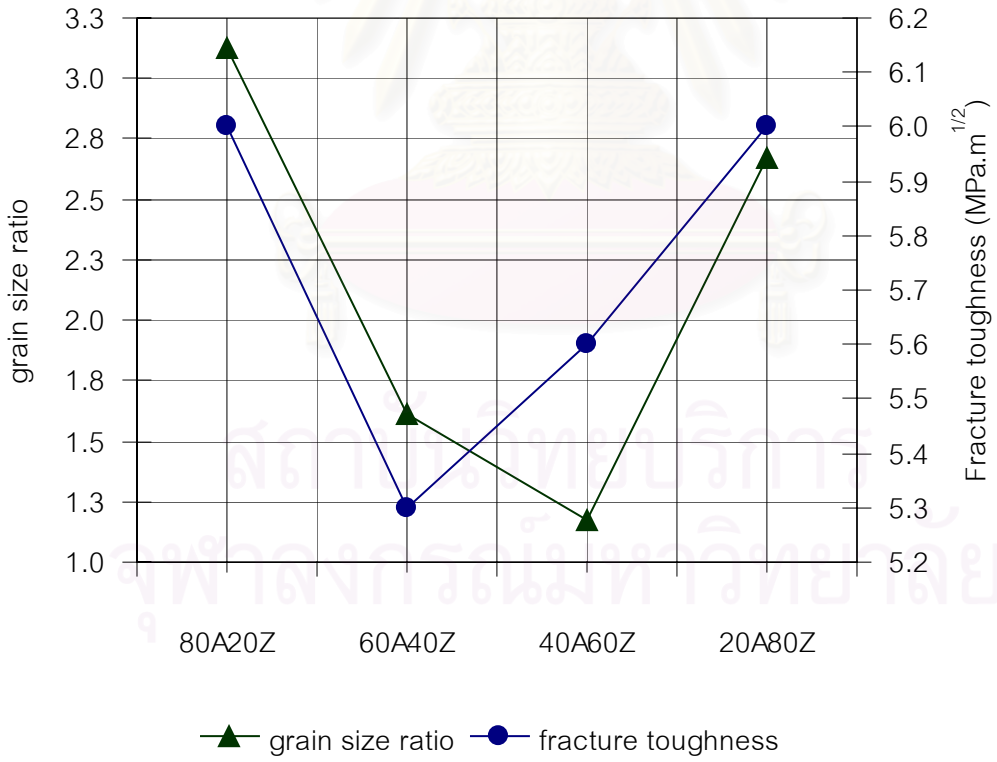

Fig.4.9 Relationship of average grain size ratio of ZrO_2:Al_2O_3 and fracture toughness

4.6 Flexural Strength Measurement

All details on the specimens for flexural strength measurement are described in Appendix 9. Fig.4.10 shows the flexural strength data as a function of weight percent of ZrO_2 content. The flexural strength of composites increases with increasing ZrO_2 content.

The average flexural strength of 20A80Z sintered at 1550^{O}C for 2 h shows the maximum value, 632 MPa. It indicates that the high ZrO_2 content causes more phase transformation hence enhances strength significantly. Moreover, this is also due to the high ZrO_2 content in 20A80Z which results in density higher than 80A20Z. However, both compositions show the same K_{1c} value. At high sintering temperature, the reduction of sintered densities of specimens appears with the grain growth. Therefore, the density of 20A80Z becomes lower at 1600^{O}C and strength is damaged. The flexural strengths of 100Z at 1550 and 1600^{O}C are the vicinity values, corresponding to the relative densities.

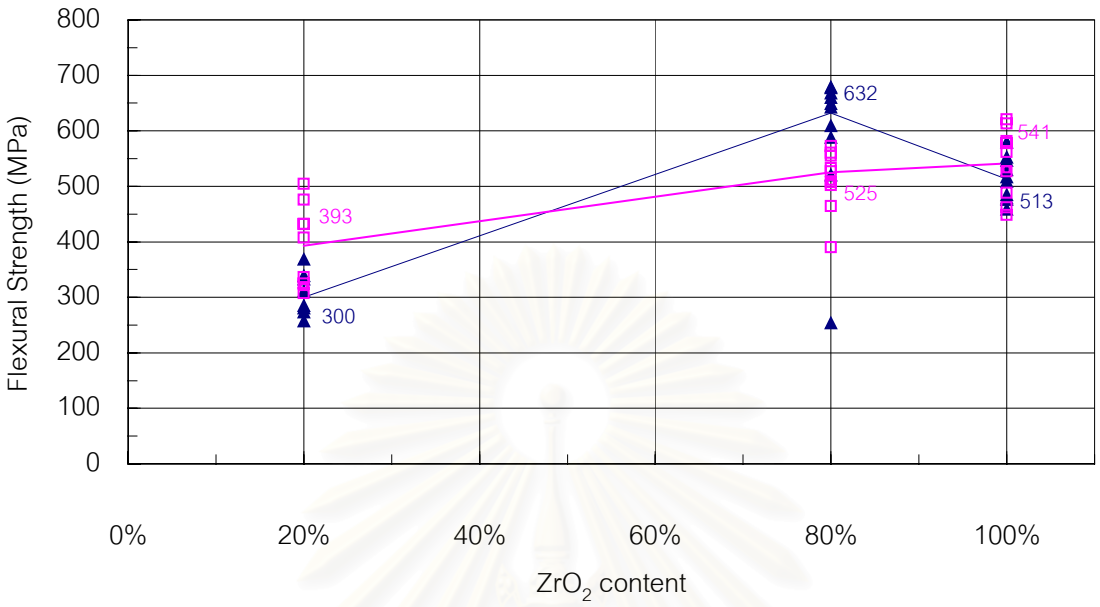

Fig.4.10 Flexural strength of Al_2O_3-ZrO_2 composite as a function of ZrO_2 content. The blue line is specimens sintered at 1550^{O}C and pink line is specimens sintered at 1600^{O}C

The SEM micrographs of fractured surfaces indicated the causes of failure are shown in Fig.4.10 and more micrographs are attached in Appendix 10. Micrographs of 20A80Z sintered at 1550^{O}C are shown in Fig.4.11 (a) and (b), and sintered at 1600^{O}C shown in Fig.4.11 (c) and (d). The Wallner lines that observed in Fig.4.11 (a) and (c) are non-uniform distance [8]. The microstructures of these materials are shown in Fig.4.11 (b) and (d). The black part is not pores, but grain pulled out. The grain size increases at 1600^{O}C and results in decrease strength. Furthermore, the grain sizes of 80A20Z sintered at 1600^{O}C are obviously larger than those at 1550^{O}C. However, the density of 80A20Z at 1550^{O}C is lower than that at 1600^{O}C. Then, the lower density might be the cause of low strength.

(a)

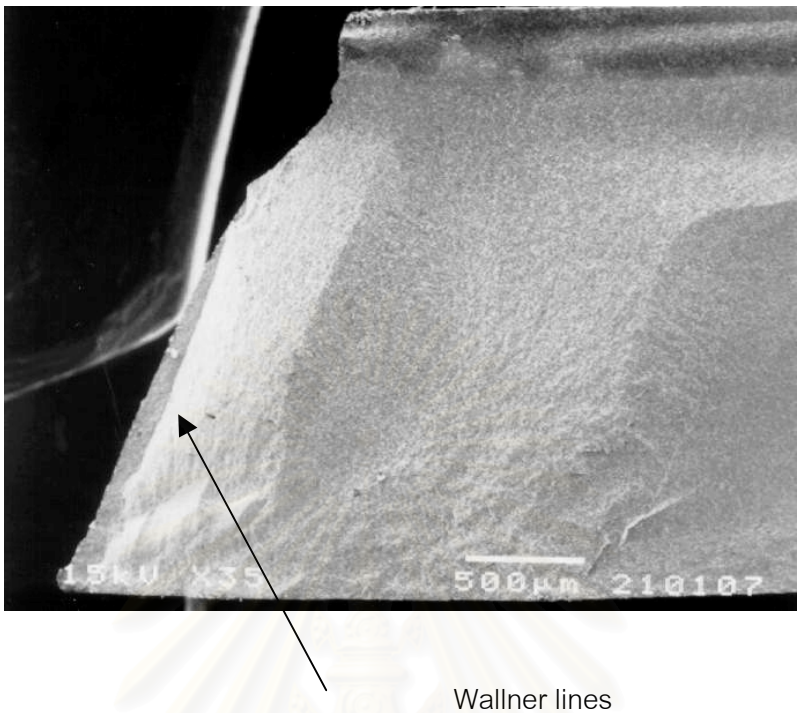

(b)

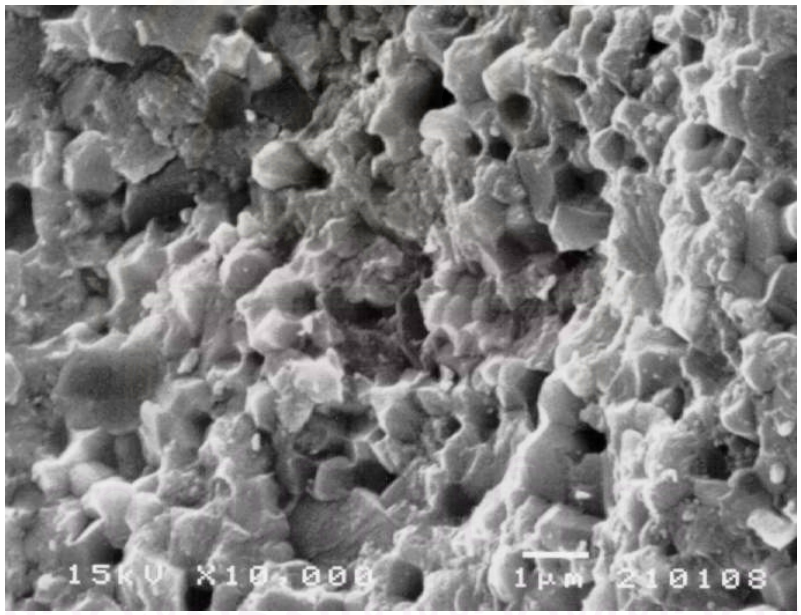

Fig.4.11 SEM micrographs of the fractured surface of 20A80Z (a) and (b) sintered at 1550^{O}C

(c)

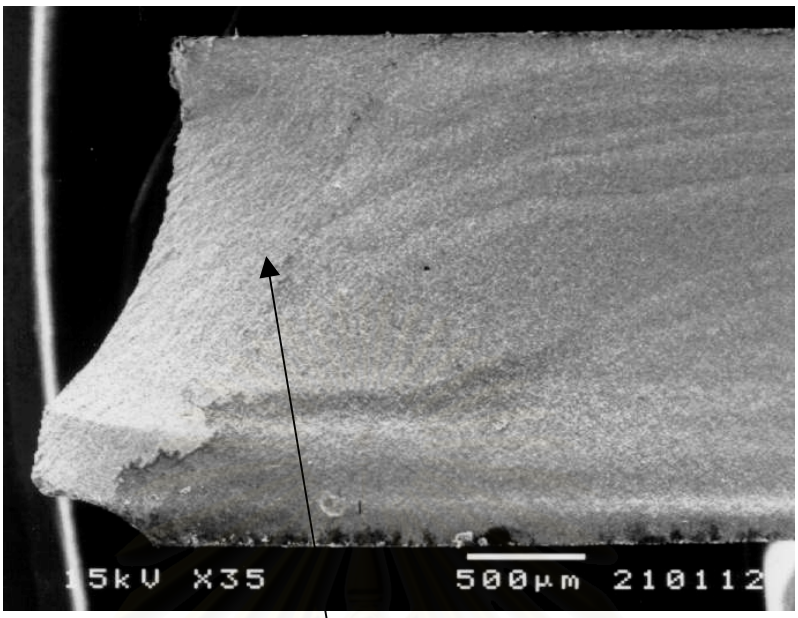

Wallner lines

(d)

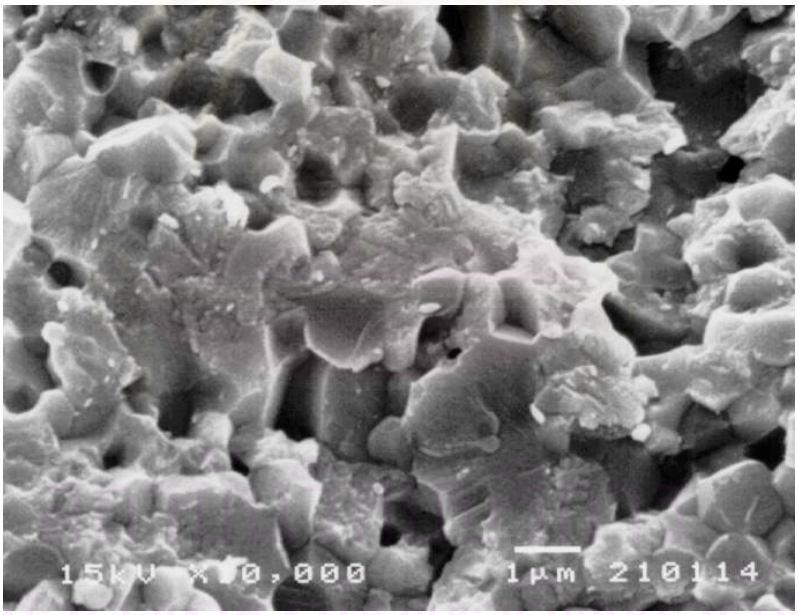

Fig.4.11 SEM micrographs of the fractured surface of 20A80Z (c) and (d) sintered at 1600^{O}C

CHAPTER 5

CONCLUSIONS

1. The average particle sizes of raw powders are reduced by attrition mill for 10 h. The average particle size at 50% cumulative of Al_2O_3 A-21 milled with Al_2O_3 balls is 0.73 μm, of ZrO_2 GTYS-5 milled with Al_2O_3 balls and ZrO_2 balls are 0.44 and 0.57 μm, respectively. These values are also ensured by specific surface area measurement.

2. Milling by attrition mill does not affect the phase of powder.

3. The relative density of Al_2O_3 A-21 milled for 10 h increases with elevating temperature and its specimens consolidate to almost full density at 1550^{O}C. Those of ZrO_2 milled with ZrO_2 balls become as high as 96-98% at 1450-1600^{O}C. They are higher than that of ZrO_2 milled with Al_2O_3 balls and as-received ZrO_2 at the same sintering temperature due to the difference of particle size and purity.

4. The relative density of alumuna-zirconia composite reaches to almost theoretical density and can be classified into two groups. The first group is high ZrO_2 content. It shows higher density at low sintering temperature, but the density decreases when sintering temperature over 1550^{O}C. The other group is high Al_2O_3 content. Its density increases with the increasing in sintering temperature. These results correspond to the tendency of the major component of composite.

5. Vickers hardness of composites increases with increase in Al_2O_3 content. 80A20Z shows the maximum hardness of 16 GPa.

6. Fracture toughness of 20A80Z and 80A20Z are the maximum at 6.0 MPa.$m^{1/2}$. It is dramatically decreases in the case of 60A40Z because the decease in average grain size of Al_2O_3. The bend of crack path decreases and the crack tends to follow the Al_2O_3 grain boundaries.

7. The flexural strength of specimen 20A80Z sintered at 1550^{O}C for 2 h shows the maximum value of 632 MPa. The small average grain size and higher relative density encourages the high strength.

CHAPTER 6

FUTURE WORK

1. In this research, a ZrO_2 particle with average grain size 0.57 μm was used. In next experiment, various average particle size ZrO_2 should be used to know the effect of particle size on hardness, fracture toughness and strength.

2. The flexural strength of specimens in this experiment was 632 MPa and not as high as 1000 MPa. It is important to make clear the practical parameters which affect the strength of Y-TZP.

3. In this experiment we did not add the additives into the composites to enhance fabrication. However, there are various types of additive that do not react with raw material which should be added to raise the relative densities of the composites.

REFERENCES

1. K.Tsukuma, K.Ueda. Strength and Fracture Toughness of Isostatically Hot-Pressed Composites of Al_2O_3 and Y2O3-Partially-Stabilized ZrO_2. J.Am.Ceram.Soc. 68[1]1985: c-4—c-5.
2. Product information. Available from: http://www.m-cera.com/English/index.e-html
3. Ceramic insert. Available from: http://www.m-cera.com/English/index.e-html
4. R. Stevens, Zirconia and Zirconia ceramics: Chemical Zirconia, second edition, pp.9-10. Leeds: Magnesium Elektron.
5. Eugene Ryshkewitch. Oxide ceramics, Physical Chemistry and Technology: Zirconia, pp.350-357. New York: Academic Press, 1960.
6. R. Stevens, Zirconia and Zirconia ceramics: Chemical Zirconia, second edition, p.10. Leeds: Magnesium Elektron.
7. M. H. Bocanegra-Bernal, S. Díaz de La Torre. Review Phase transformations of zirconium dioxide and related materials for high performance engineering ceramics. J. Mats. Sci. 37(2002): 4947-4971.
8. David W. Richerson, Modern Ceramic Engineering, Properties, Processing and use in Design: Polymorphic Forms and Transformations, pp.18-19. New York: Marcel Dekker, 1982.
9. Michel Barsoum, Fundamentals of Ceramics: One Component Systems, international edition, pp. 267-269. Singapore: McGraw-HILL, 1997.
10. Engineering Ceramics: Zirconia. Available from: http://users.ox.ac.uk/~roberts/sgrgroup/lectures/introceram/4examples.pdf
11. Richard H. J. Hannink, Patric M. Kelly, Barry C. Muddle. Transformation Toughening in Zirconia-Containing Ceramics. J. Am. Ceram. Soc. 83[3]2000: 461-87.
12. Material: Zirconia Ceramic. Available from: http://www.JFCC.or.jp/05-material/ceram.html.
13. W. H. Tuan, R. Z. Chen, T. C. Wang, C. H. Cheng, P.S. Kuo. Mechanical properties of Al_2O_3/ZrO_2 composites. J. Eur. Ceram. Soc. 22(2002): 2827-2833.

14. G. K. Bansal, A. H. Heuer. Precipitation in Partially Stabilized Zirconia. J.Am.Ceram.Soc. 58[5-6]1975: 235-238.

15. A.G. Evans, A. H. Heuer. Review-Transformation Toughening in Ceramics: Martensitic Transformation in Crack-Tip Stress Field. J. Am. Ceram. Soc. 63[5-6](1980): 241-44

16. Roy W. Rice, Ceramic Fabrication Technology:Polymorphic form and transformation pp.152-153. New York: Marcel Dekker, 2003.

17. Patrick M. Kelly, L. R. Francis Rose. The Martensitic Transformation in Ceramics-its Role in Transformation Toughening. Progress in Materials Science. 47(2002): 463-557.

18. N. Claussen. Fracture Toughness of Al_2O_3 with an Unstabilized ZrO_2 Dispersed Phase. J.Am.Ceram.Soc. 59[1-2] 1976: 49-51.

19. Yu-Seon Shin, Young-Woo Rhee, Suk-Joong L. Kang. Experimental Evaluation of Toughening Mechanisms in Alumina-Zirconia Composites. J.Am.Ceram.Soc. 82[5]1999: 1229-1232.

20. B. Smuk, M. Szutkowska, J. Walter. Alumina ceramics with partially stabilized zirconia for cutting tools. J.Mats.Proc.Tech. 133 (2003): 195-198.

21. S. N. B. Hodgson, J. Cawley, M. Clubley. The role of Al_2O_3 impurities on the microstructure and properties of Y-TZP. J. Mats. Proc.,Tech. 92-93 (1999): 85-90.

22. Jue Wang, Eric M. Taleff, Desiderio Kovar. High-temperature deformation of Al_2O_3/Y-TZP particle composites. Acta Materiallia. 51 (2003): 3571-3583.

23. Annamaria Celli, Antonella Tucci, Leonardo Esposito, Carlo Palmonari. Fractal analysis of cracks in alumina-zirconia composites. J.Eur.Ceram.Soc. 23(2003): 469-479.

APPENDICES

Appendix 1

The condition for attrition mill

Type of powder	Al_2O_3 A-21	ZrO_2 GTYS-5	ZrO_2 GTYS-5
Type of balls	Al_2O_3	Al_2O_3	ZrO_2
Ball diameter (mm.)	3	3	5
Rotor speed (rpm.)	550	550	550
Milling time (h.)	10	10	10
Weight of powder (g)	215	200	200
Volume of water (cm^3)	170	170	170
Weight of balls (g)	1215.54	1215.58	1657.18
Weight of dry balls (g)	1177.2	1170.32	1648.99
Wear of balls (g)	38.34	45.26	8.69

Appendix 2

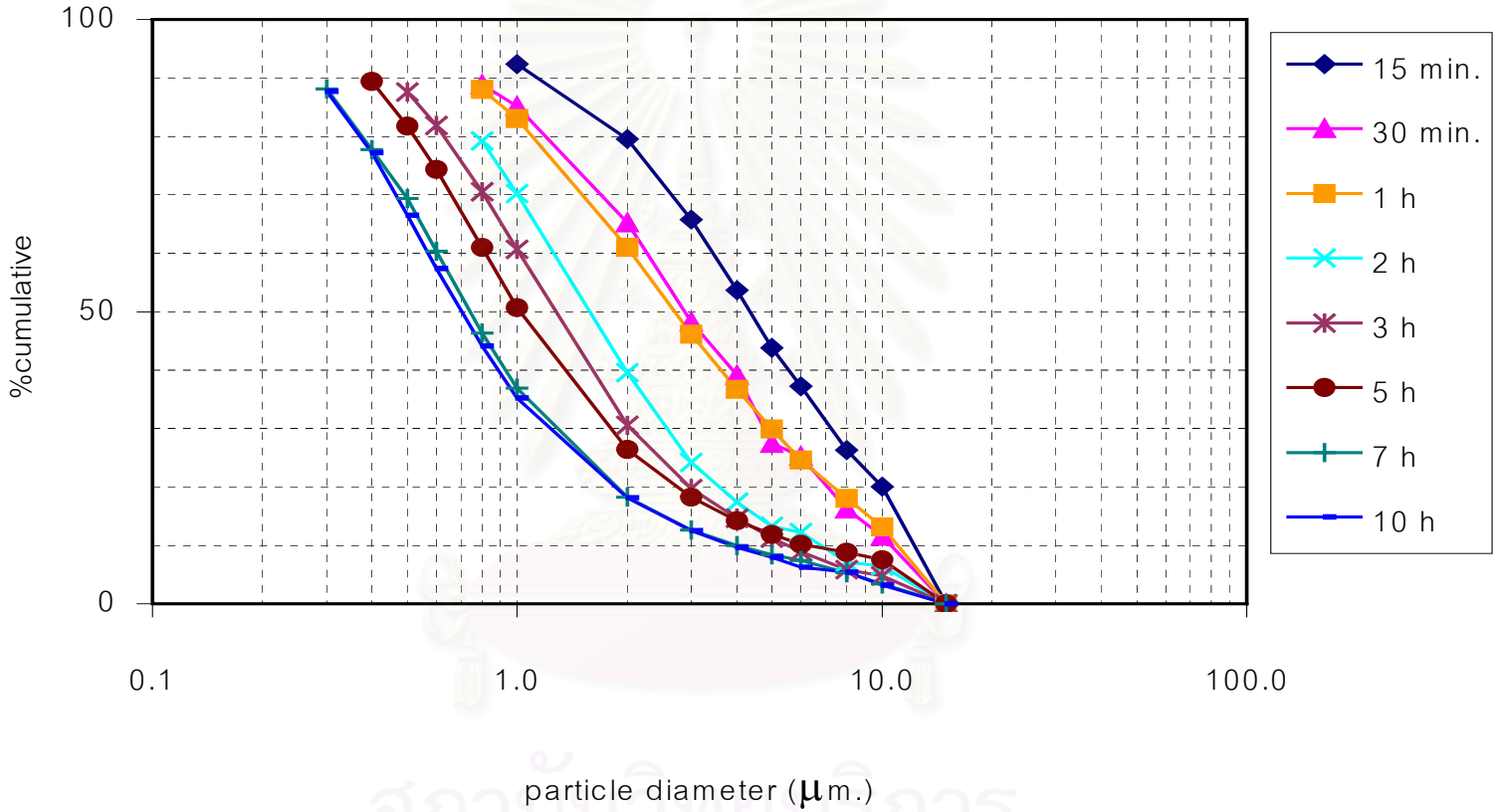

Particle size distribution of A-21with Al_2O_3 balls sampling at various periods of times of milling

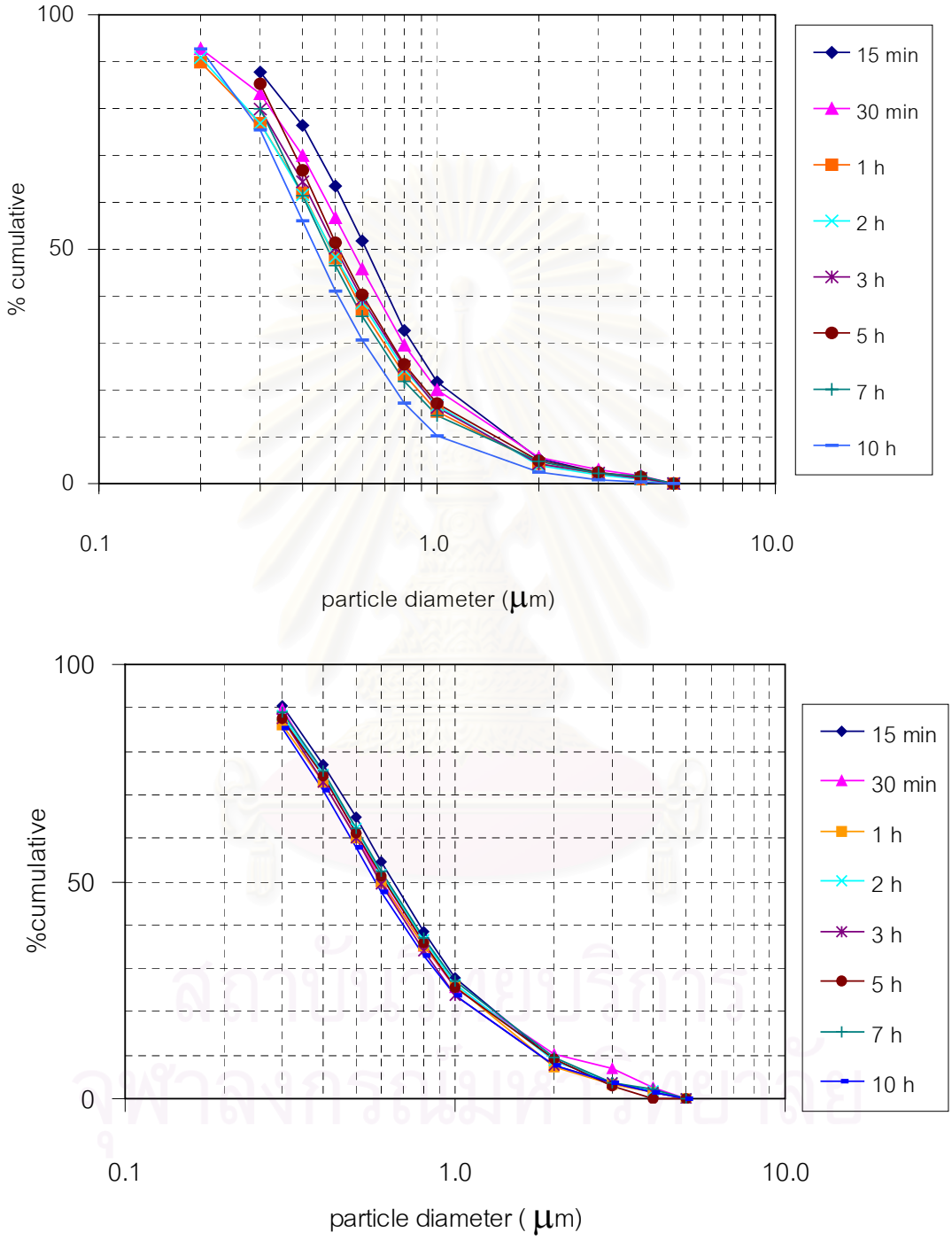

Particle size distribution of GTYS-5 with Al_2O_3 balls (upper figure) and ZrO_2 balls (lower figure) sampling at various periods of times of milling

Appendix 3

Percent of theoretical density (%TD) of alumina A-21 (milled for 10 h with Al_2O_3 balls) as a function of sintering temperature.

sintering temp. (^{O}C)	W_{sus} (g)	W_{sat} (g)	W_d (g)	water absorption (%)	density (g/cm^3)	% TD	linear shrinkage (%)
1350	2.3790	3.5456	3.1984	10.86	2.73	69.22	14.51
	2.3717	3.5328	3.1848	10.93	2.74	69.26	14.10
	2.4106	3.5886	3.2385	10.81	2.74	69.41	15.34
	2.4011	3.5798	3.2225	11.09	2.73	69.03	15.39
	2.4052	3.5784	3.2242	10.99	2.74	69.39	14.99
average	2.3935	3.5650	3.2137	10.93	2.74	69.26	14.87
1400	2.4710	3.5839	3.3115	8.23	2.97	75.13	10.38
	2.4885	3.6111	3.3342	8.30	2.96	74.99	11.16
	2.4858	3.6203	3.3404	8.38	2.94	74.34	12.09
	2.4738	3.5963	3.3195	8.34	2.95	74.67	11.15
	2.4826	3.6220	3.3369	8.54	2.92	73.94	12.47
average	2.4803	3.6067	3.3285	8.36	2.95	74.61	11.45
1450	2.3792	3.3074	3.1835	3.89	3.42	86.53	16.52
	2.3829	3.3286	3.1998	4.03	3.37	85.36	16.51
	2.3918	3.3341	3.2067	3.97	3.39	85.85	16.50
	2.3726	3.3187	3.1898	4.04	3.36	85.06	16.33
	2.3932	3.3486	3.2153	4.15	3.35	84.90	16.24
average	2.3839	3.3275	3.1990	4.02	3.38	85.53	16.42
1500	2.3871	3.2980	3.2168	2.52	3.52	89.12	17.54
	2.3430	3.2246	3.1612	2.01	3.57	90.49	17.90
	2.3679	3.2574	3.2006	1.77	3.59	90.80	18.05
	2.3420	3.2213	3.1663	1.74	3.59	90.87	18.01
	2.3482	3.2290	3.1739	1.74	3.59	90.94	17.98
average	2.3576	3.2461	3.1838	1.96	3.57	90.44	17.90

sintering temp. (^{O}C)	W_{sus} (g)	W_{sat} (g)	W_d (g)	water absorption (%)	density (g/cm^3)	%TD	linear shrinkage (%)
1550	2.4351	3.3010	3.2995	0.05	3.80	96.16	20.32
	2.4290	3.2887	3.2861	0.08	3.81	96.46	20.35
	2.3374	3.1717	3.1674	0.14	3.78	95.81	19.67
	2.3354	3.1744	3.1705	0.12	3.77	95.36	19.53
	2.3327	3.1693	3.1671	0.07	3.77	95.53	19.68
average	2.3740	3.2210	3.218	0.09	3.79	95.87	19.91
1600	2.4225	3.2795	3.2739	0.17	3.81	96.41	20.82
	2.4532	3.3188	3.3160	0.08	3.82	96.67	20.83
	2.4393	3.3010	3.2987	0.07	3.82	96.61	20.80
	2.4370	3.3010	3.2993	0.05	3.81	96.37	20.80
	2.4290	3.2923	3.2897	0.08	3.80	96.16	20.86
average	2.436	3.299	3.296	0.09	3.81	96.44	20.82
1650	2.3609	3.1840	3.1826	0.04	3.85	97.58	20.07
	2.3641	3.1968	3.1955	0.04	3.83	96.84	19.72
	2.3723	3.2070	3.2058	0.04	3.83	96.92	19.76
	2.3591	3.1876	3.1867	0.03	3.83	97.07	19.86
	2.3519	3.1806	3.1801	0.02	3.83	96.84	19.84
average	2.3617	3.1912	3.1901	0.03	3.83	97.05	19.85

Percent of theoretical density (%TD) of zirconia GTYS-5 (milled for 10 h with Al_2O_3 balls) as a function of sintering temperature.

sintering temp. (^{O}C)	W_{sus} (g)	W_{sat} (g)	W_d (g)	water absorption (%)	density (g/cm^3)	%TD	linear shrinkage (%)
1350	2.6626	3.3144	3.3115	0.09	5.07	92.23	22.45
	2.6216	3.2616	3.2560	0.17	5.07	92.35	22.65
	2.6670	3.3213	3.3170	0.13	5.06	92.03	22.65
	2.7031	3.3662	3.3600	0.18	5.05	91.98	22.44
	2.6510	3.3048	3.2966	0.25	5.03	91.53	22.49
average	2.6611	3.3137	3.3082	0.16	5.06	92.02	22.54
1400	2.6485	3.2723	3.2699	0.07	5.23	95.11	23.19
	2.6610	3.2890	3.2871	0.06	5.22	94.97	23.22
	2.6409	3.2654	3.2639	0.05	5.21	94.83	23.48
	2.6445	3.2720	3.2697	0.07	5.19	94.54	23.38
	2.6549	3.2838	3.2816	0.07	5.20	94.67	23.44
average	2.6500	3.2765	3.2744	0.06	5.21	94.82	23.34
1450	2.7006	3.3424	3.3412	0.04	5.19	94.43	23.12
	2.6815	3.3188	3.3166	0.07	5.19	94.39	22.90
	2.6990	3.3381	3.3370	0.03	5.20	94.71	23.22
	2.6964	3.3375	3.3362	0.04	5.19	94.39	22.98
	2.7024	3.3419	3.3404	0.04	5.21	94.74	23.22
average	2.6960	3.3357	3.3343	0.04	5.19	94.53	23.09
1500	2.7119	3.3528	3.3519	0.03	5.21	94.89	22.87
	2.7085	3.3504	3.3486	0.05	5.20	94.65	22.75
	2.7046	3.3489	3.3460	0.09	5.18	94.22	22.91
	2.6748	3.3118	3.3093	0.08	5.18	94.26	22.80
	2.6936	3.3375	3.3349	0.08	5.16	93.97	22.97
average	2.6987	3.3403	3.3381	0.06	5.19	94.40	22.86

sintering temp. (^{O}C)	W_{sus} (g)	W_{sat} (g)	W_d (g)	water absorption (%)	density (g/cm^3)	%TD	linear shrinkage (%)
1550	2.6369	3.2952	3.2940	0.04	4.99	90.79	22.02
	2.6442	3.3042	3.3027	0.05	4.99	90.79	21.99
	2.6561	3.3159	3.3146	0.04	5.01	91.15	22.09
	2.6585	3.3183	3.3164	0.06	5.01	91.20	22.07
	2.6598	3.3164	3.3145	0.06	5.03	91.59	22.20
average	2.6511	3.3100	3.3084	0.05	5.01	91.10	22.07
1600	2.6056	3.3232	3.3223	0.03	4.61	84.00	19.88
	2.5705	3.2913	3.2894	0.06	4.55	82.80	20.05
	2.5926	3.3121	3.3107	0.04	4.59	83.49	20.07
	2.6044	3.3124	3.3114	0.03	4.66	84.86	20.07
	2.6001	3.3114	3.3096	0.05	4.64	84.42	20.14
average	2.5946	3.3101	3.3087	0.04	4.61	83.91	20.04
1650	2.6043	3.3843	3.3819	0.07	4.32	78.67	18.24
	2.5862	3.3663	3.3642	0.06	4.30	78.24	18.12
	2.5999	3.3737	3.3711	0.08	4.34	79.04	18.41
	2.5944	3.3708	3.3693	0.04	4.33	78.74	18.07
	2.5755	3.3439	3.3424	0.04	4.34	78.92	18.58
average	2.5921	3.3678	3.3658	0.06	4.32	78.72	18.29

Percent of theoretical density %TD of zirconia GTYS-5 (milled for 10 h with ZrO_2 balls) as a function of sintering temperature.

sintering temp. (^{O}C)	W_{sus} (g)	W_{sat} (g)	W_d (g)	water absorption (%)	density (g/cm^3)	%TD	linear shrinkage (%)
1350	2.6860	3.3274	3.2386	2.74	5.03	83.89	20.70
	2.6797	3.3152	3.2264	2.75	5.06	84.35	20.67
	2.6742	3.3174	3.2209	3.00	4.99	83.19	20.64
average	2.6800	3.3200	3.2286	2.83	5.03	83.81	20.67
1400	2.6548	3.2350	3.2253	0.30	5.54	92.35	23.43
	2.6476	3.2223	3.2126	0.30	5.57	92.87	23.31
	2.6609	3.2374	3.2252	0.38	5.58	92.94	23.31
average	2.6544	3.2316	3.2210	0.33	5.56	92.72	23.35
1450	2.6810	3.2340	3.2334	0.02	5.83	97.17	24.58
	2.6852	3.2388	3.2378	0.03	5.83	97.19	24.37
	2.6768	3.2305	3.2284	0.07	5.81	96.89	24.21
average	2.6810	3.2344	3.2332	0.04	5.83	97.08	24.38
1500	2.6917	3.2400	3.2383	0.05	5.89	98.09	24.51
	2.7023	3.2524	3.2512	0.04	5.89	98.16	24.45
	2.6941	3.2430	3.2414	0.05	5.88	98.08	24.30
average	2.6960	3.2451	3.2436	0.05	5.89	98.11	24.42
1550	2.7371	3.2985	3.2978	0.02	5.86	97.62	23.98
	2.6835	3.2358	3.2341	0.05	5.84	97.31	23.79
	2.7168	3.2743	3.2737	0.02	5.85	97.58	23.89
average	2.7125	3.2695	3.2685	0.03	5.85	97.50	23.89
1600	2.6973	3.2608	3.2603	0.02	5.77	96.15	23.80
	2.7167	3.2868	3.2861	0.02	5.75	95.79	23.91
	2.7228	3.2921	3.2910	0.03	5.76	96.07	23.60
average	2.7123	3.2799	3.2791	0.02	5.76	96.00	23.77

sintering temp. (^{O}C)	W_{sus} (g)	W_{sat} (g)	W_{d} (g)	water absorption (%)	density (g/cm^{3})	%TD	linear shrinkage (%)
1650	2.3747	2.8932	2.8927	0.02	5.57	92.76	24.75
	2.4299	2.9511	2.9509	0.01	5.65	94.13	24.75
	2.4116	2.9278	2.9270	0.03	5.66	94.28	24.75
average	2.4054	2.9240	2.9235	0.02	5.62	93.72	24.75

Percent of theoretical density (%TD) of zirconia GTYS-5 (as-received) as a function of sintering temperature.

sintering temp. (^{O}C)	W_{sus} (g)	W_{sat} (g)	W_d (g)	water absorption (%)	density (g/cm^3)	%TD	linear shrinkage (%)
1350	2.7610	3.5546	3.3217	7.01	4.17	69.57	11.98
	2.7660	3.5604	3.3240	7.11	4.17	69.55	11.99
	2.7779	3.5825	3.3405	7.24	4.14	69.01	12.00
	2.7867	3.5937	3.3516	7.22	4.14	69.03	11.91
	2.7560	3.5599	3.3157	7.36	4.11	68.56	11.79
average	2.7695	3.5702	3.3307	7.19	4.15	69.14	11.93
1400	2.6886	3.3577	3.2253	4.11	4.80	80.08	15.49
	2.6963	3.3772	3.2397	4.24	4.74	79.05	15.68
	2.7128	3.4062	3.2613	4.44	4.69	78.14	15.66
	2.6983	3.3793	3.2409	4.27	4.74	79.06	15.52
	2.6928	3.3743	3.2376	4.22	4.74	78.93	15.53
average	2.6978	3.3789	3.2410	4.26	4.74	79.04	15.58
1450	2.7147	3.3389	3.2616	2.37	5.21	86.85	18.20
	2.6714	3.2820	3.2103	2.23	5.24	87.39	18.03
	2.7004	3.3188	3.2466	2.22	5.24	87.27	17.87
	2.6996	3.3158	3.2461	2.15	5.25	87.56	17.84
	2.6716	3.2884	3.2129	2.35	5.20	86.58	17.83
average	2.6915	3.3088	3.2355	2.26	5.23	87.13	17.95
1500	2.6688	3.2739	3.2319	1.30	5.33	88.78	20.03
	2.6383	3.2215	3.2006	0.65	5.47	91.22	19.43
	2.6544	3.2408	3.2219	0.59	5.48	91.33	19.30
	2.6345	3.2185	3.1971	0.67	5.46	91.00	19.31
	2.6399	3.2205	3.2020	0.58	5.50	91.67	19.37
average	2.6472	3.2350	3.2107	0.76	5.45	90.78	19.49

sintering temp. (^{O}C)	W_{sus} (g)	W_{sat} (g)	W_d (g)	water absorption (%)	density (g/cm^3)	relative density (%)	linear shrinkage (%)
1550	2.6716	3.2505	3.2430	0.23	5.59	93.09	20.40
	2.7161	3.2977	3.2965	0.04	5.65	94.19	20.37
	2.7214	3.3040	3.3004	0.11	5.65	94.14	20.65
	2.7309	3.3151	3.3134	0.05	5.66	94.25	20.49
	2.7630	3.3549	3.3512	0.11	5.65	94.09	20.35
average	2.7206	3.3044	3.3009	0.11	5.64	93.95	20.45
1600	2.6301	3.1984	3.1977	0.02	5.61	93.53	20.10
	2.6317	3.2010	3.1999	0.03	5.61	93.43	19.97
	2.6783	3.2570	3.2560	0.03	5.61	93.52	20.30
	2.6631	3.2401	3.2390	0.03	5.60	93.31	19.87
	2.6451	3.2164	3.2153	0.03	5.61	93.55	20.11
average	2.6497	3.2226	3.2216	0.03	5.61	93.47	20.07
1650	2.6080	3.1734	3.1712	0.07	5.59	93.18	19.32
	2.6068	3.1748	3.1725	0.07	5.57	92.79	19.57
	2.6421	3.2162	3.2145	0.05	5.58	93.02	20.03
	2.6367	3.2084	3.2063	0.07	5.59	93.17	20.13
	2.6332	3.2024	3.2008	0.05	5.61	93.42	19.88
average	2.6254	3.1950	3.1931	0.06	5.59	93.12	19.79

Percent of theoretical density (%TD) and sintering temperature of all specimens in preliminary sintering.

powder	Theoretical density (g/cm^3)	sintering temp. (^OC)	Average density (g/cm^3)		%TD		% linear shrinkage	
			non CIP	CIP	non CIP	CIP	non CIP	CIP
Al_2O_3 (A-21)	3.95	1350	2.736		69.262		9.706	
		1400	2.947		74.615		12.815	
		1450	3.379		85.539		16.419	
		1500	3.573		90.444		17.898	
		1550	3.787		95.865		19.911	
		1600	3.809		96.443		20.822	
		1650	3.832		97.001		19.850	
ZrO_2 (GTYS-5) as-received	6.00	1350	4.149		69.146		11.932	
		1400	4.743		79.052		15.576	
		1450	5.228		87.133		17.953	
		1500	5.448		90.800		19.489	
		1550	5.637		93.953		20.454	
		1600	5.608		93.468		20.072	
		1650	5.587		93.119		19.787	
ZrO_2 (GTYS-5) milled 10 h. used Al_2O_3 balls	5.49	1350	5.056		92.025		22.536	
		1400	5.210		94.823		23.342	
		1450	5.194		94.531		23.087	
		1500	5.186		94.399		22.860	
		1550	5.005		91.102		22.073	
		1600	4.610		83.913		20.043	
		1650	4.325		78.723		18.285	

powder	Theoretical density (g/cm^3)	sintering temp. (^OC)	Average density (g/cm^3)		%TD		% linear shrinkage	
			non CIP	CIP	non CIP	CIP	non CIP	CIP
ZrO_2 (GTYS-5) milled 10 h used ZrO_2 balls	6.00	1350	5.029	5.153	83.809	85.877	20.668	20.998
		1400	5.563	5.458	92.722	90.959	23.350	22.701
		1450	5.825	5.763	97.084	96.055	24.384	24.251
		1500	5.887	5.829	98.108	97.157	24.420	24.572
		1550	5.850	5.775	97.504	96.253	23.888	24.221
		1600	5.760	5.720	96.000	95.333	23.770	24.010
		1650						
ZrO_2 (TZ-3Y20A)	6.00	1350	4.790		79.828		18.073	
		1400	5.140		85.673		20.354	
		1450	5.339		88.978		21.536	
		1500	5.414		90.233		21.780	
		1550	5.401		90.014		21.764	
		1600	5.434		90.563		21.900	
		1650						

Appendix 4

Percent of theoretical density (%TD) of 80A20Z as a function of sintering temperature.

sintering temperature (^{O}C)	W_{sus} (g)	W_{sat} (g)	W_d (g)	water absorption (%)	density (g/cm^3)	%TD	linear shrinkage (%)
1500	2.1855	2.9846	2.8616	4.30	3.57	84.17	19.99
	2.1893	2.9833	2.8641	4.16	3.59	84.78	20.01
	2.1887	2.9886	2.8633	4.38	3.57	84.13	20.01
average	2.1878	2.9855	2.8630	4.28	3.58	84.36	20.00
1550	2.1598	2.8693	2.8612	0.28	4.02	94.78	19.56
	2.1664	2.8692	2.8628	0.22	4.06	95.74	19.57
	2.1670	2.8741	2.8632	0.38	4.04	95.17	19.74
average	2.1644	2.8709	2.8624	0.30	4.04	95.23	19.62
1600	2.1768	2.8642	2.8620	0.08	4.15	97.91	20.42
	2.1778	2.8623	2.8608	0.05	4.17	98.28	20.21
	2.1766	2.8611	2.8593	0.06	4.17	98.23	20.73
average	2.1771	2.8625	2.8607	0.06	4.16	98.14	20.45
1650	2.1780	2.8626	2.8607	0.07	4.17	98.26	20.13
	2.1764	2.8626	2.8608	0.06	4.16	98.04	20.26
	2.1782	2.8626	2.8593	0.12	4.17	98.24	20.13
average	2.1775	2.8626	2.8603	0.08	4.16	98.18	20.17

Percent of theoretical density (%TD) of 60A40Z as a function of sintering temperature.

sintering temp. (^{O}C)	W_{sus} (g)	W_{sat} (g)	W_d (g)	water absorption (%)	density (g/cm^3)	%TD	linear shrinkage (%)
1500	2.2282	2.9492	2.8533	3.36	3.94	86.20	20.80
	2.2322	2.9746	2.8564	4.14	3.83	83.81	20.55
	2.2412	2.9860	2.8681	4.11	3.84	83.88	20.80
average	2.2339	2.9699	2.8593	3.87	3.87	84.61	20.72
1550	2.2184	2.8658	2.8611	0.16	4.40	96.26	20.27
	2.2163	2.8673	2.8620	0.19	4.38	95.76	20.21
	2.2153	2.8660	2.8611	0.17	4.38	95.78	20.27
average	2.2167	2.8664	2.8614	0.17	4.39	95.93	20.25
1600	2.2321	2.8702	2.8679	0.08	4.48	97.95	21.18
	2.2250	2.8604	2.8591	0.05	4.49	98.07	21.00
	2.2255	2.8606	2.8590	0.06	4.49	98.11	21.12
average	2.2275	2.8637	2.8620	0.06	4.49	98.04	21.10
1650	2.2241	2.8689	2.8679	0.03	4.43	96.93	20.80
	2.2245	2.8653	2.8591	0.22	4.45	97.24	21.09
	2.2210	2.8601	2.8590	0.04	4.46	97.49	21.39
average	2.2232	2.8648	2.8620	0.10	4.45	97.22	21.09

Percent of theoretical density (%TD) of 40A60Z as a function of sintering temperature.

sintering temp. (^{O}C)	W_{sus} (g)	W_{sat} (g)	W_{d} (g)	water absorption (%)	density (g/cm^{3})	%TD	linear shrinkage (%)
1500	2.2800	2.9145	2.8714	1.50	4.51	90.76	19.22
	2.2824	2.9197	2.8788	1.42	4.50	90.59	19.54
	2.2820	2.9276	2.8745	1.85	4.44	89.29	19.36
average	2.2815	2.9206	2.8749	1.59	4.48	90.21	19.37
1550	2.2868	2.8762	2.8750	0.04	4.86	97.83	21.52
	2.2876	2.8771	2.8755	0.06	4.86	97.83	21.57
	2.2907	2.8833	2.8811	0.08	4.84	97.50	21.76
average	2.2884	2.8789	2.8772	0.06	4.86	97.72	21.62
1600	2.2911	2.8827	2.8811	0.06	4.86	97.72	20.00
	2.2925	2.8839	2.8822	0.06	4.86	97.79	19.95
	2.2910	2.8814	2.8798	0.06	4.86	97.88	19.98
average	2.2915	2.8827	2.8810	0.06	4.86	97.80	19.98
1650	2.2798	2.8788	2.8811	-0.08	4.80	96.51	21.52
	2.2813	2.8812	2.8822	-0.03	4.79	96.40	21.34
	2.2791	2.8784	2.8798	-0.05	4.79	96.42	21.70
average	2.2801	2.8795	2.8810	-0.05	4.79	96.44	21.52

Percent of theoretical density (%TD) of 20A80Z as a function of sintering temperature.

sintering temperature (^{O}C)	W_{sus} (g)	W_{sat} (g)	W_d (g)	water absorption (%)	density (g/cm^3)	%TD	linear shrinkage (%)
1500	2.3375	2.8870	2.8856	0.05	5.23	96.27	18.10
	2.3443	2.8953	2.8939	0.05	5.23	96.28	18.38
	2.3392	2.8915	2.8903	0.04	5.22	95.94	18.10
average	2.3403	2.8913	2.8899	0.05	5.23	96.16	18.20
1550	2.3523	2.8930	2.8916	0.05	5.33	98.04	22.48
	2.3512	2.8935	2.8914	0.07	5.31	97.74	22.42
	2.3532	2.8957	2.8937	0.07	5.32	97.78	22.61
average	2.3522	2.8941	2.8922	0.06	5.32	97.85	22.51
1600	2.3459	2.8945	2.8930	0.05	5.26	96.73	22.24
	2.3499	2.9001	2.8991	0.03	5.25	96.65	22.42
	2.3433	2.8923	2.8909	0.05	5.25	96.59	22.32
average	2.3464	2.8956	2.8943	0.04	5.25	96.65	22.32
1650	2.3323	2.8962	2.8930	0.11	5.12	94.10	21.76
	2.3288	2.8923	2.8991	-0.23	5.13	94.36	21.57
	2.3296	2.8931	2.8909	0.08	5.12	94.10	22.37
average	2.3302	2.8939	2.8943	-0.02	5.12	94.19	21.90

Relationship of the average percent of theoretical density (%TD) and sintering temperature of all specimens used in sintering of composite.

composition	Theoretical density (g/cc)	sintering temp (^{O}C)	Average density (g/cc)	%TD	%linear shrinkage
100A	3.95	1500	3.56	90.22	17.90
		1550	3.78	95.80	19.91
		1600	3.82	96.75	20.82
		1650	3.83	97.03	19.85
80A20Z	4.24	1500	3.58	84.36	18.20
		1550	4.04	95.23	22.51
		1600	4.16	98.14	22.32
		1650	4.16	98.18	21.90
60A40Z	4.58	1500	3.87	84.63	19.37
		1550	4.39	95.93	21.62
		1600	4.49	98.04	21.64
		1650	4.46	97.43	21.52
40A20Z	4.97	1500	4.48	90.22	20.72
		1550	4.86	97.72	20.25
		1600	4.86	97.80	21.10
		1650	4.79	96.45	21.09
20A80Z	5.44	1500	5.23	96.16	20.00
		1550	5.32	97.86	19.62
		1600	5.25	96.65	20.45
		1650	5.12	94.19	20.17
100Z	6.00	1500	5.89	98.11	24.42
		1550	5.85	97.50	23.89
		1600	5.76	96.00	23.77
		1650	-	-	

Appendix 5

Average grain size of Al_2O_3 and ZrO_2 for various compositions sintered at 1600^{O}C for 2 h

composition	Al_2O_3 grain size (μm)			ZrO_2 grain size (μm)			Grain size ratio ZrO_2:Al_2O_3	relative density (%)	H_v (GPa)	K_{1c} (MPa.m$^{1/2}$)
	max.	min.	avg.	max.	min.	avg.				
80A20Z	9.3	0.5	2.5	3.6	0.9	0.8	0.32	98.14	15.95	6.0
60A40Z	9.6	0.5	2.1	5.6	0.8	1.3	0.62	98.04	15.12	5.3
40A60Z	7.5	0.4	1.8	7.5	1.0	2.1	1.17	97.80	14.09	5.6
20A80Z	4.8	0.4	0.9	7.3	0.2	2.4	2.67	96.65	12.39	6.0

Appendix 6

Grain size distributions of (a) 80A20Z, (b) 60A40Z, (c) 40A60Z, and (d) 20A80Z specimens that sintered at 1600^{O}C for 2 h. A and Z is referred to Al_2O_3 and ZrO_2 grains, respectively.

(a)

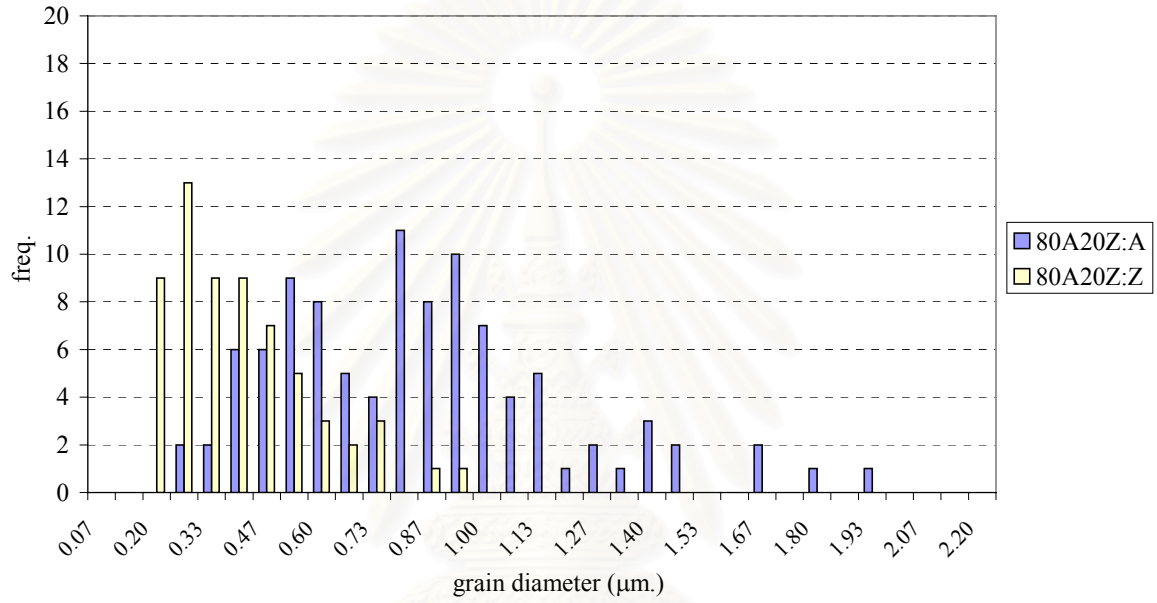

(b)

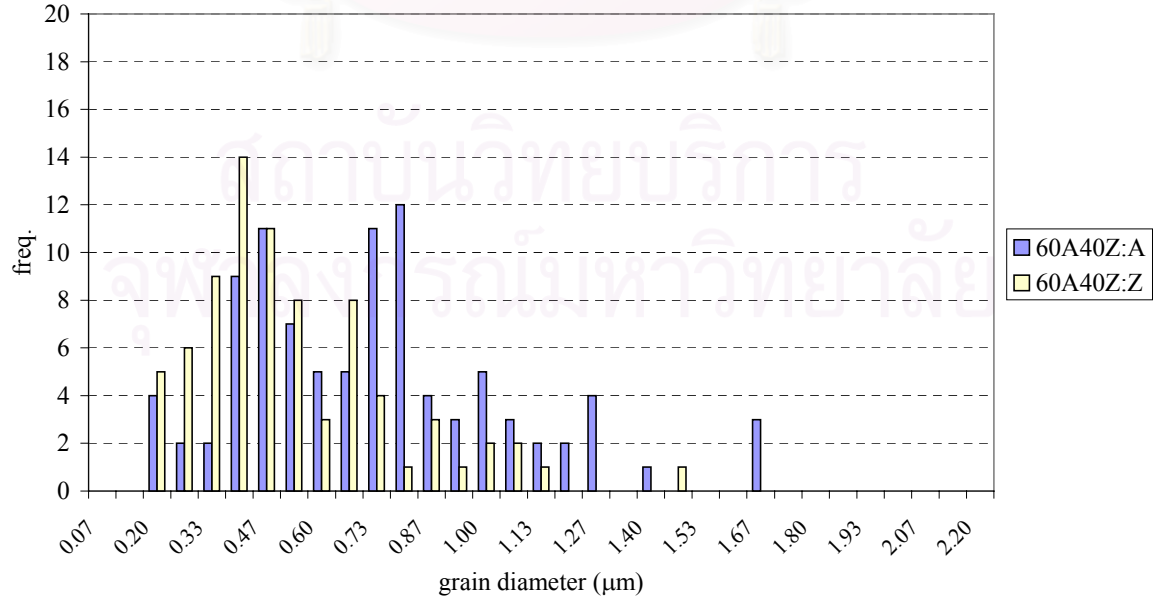

(c)

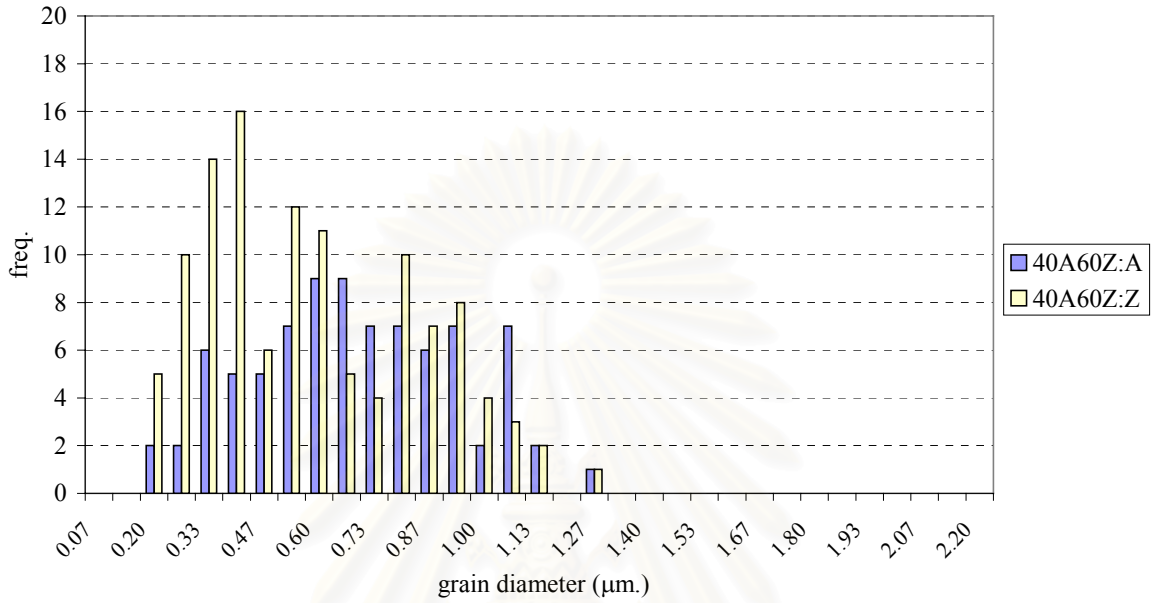
freq.
grain diameter (μm.)
40A60Z:A
40A60Z:Z

(d)

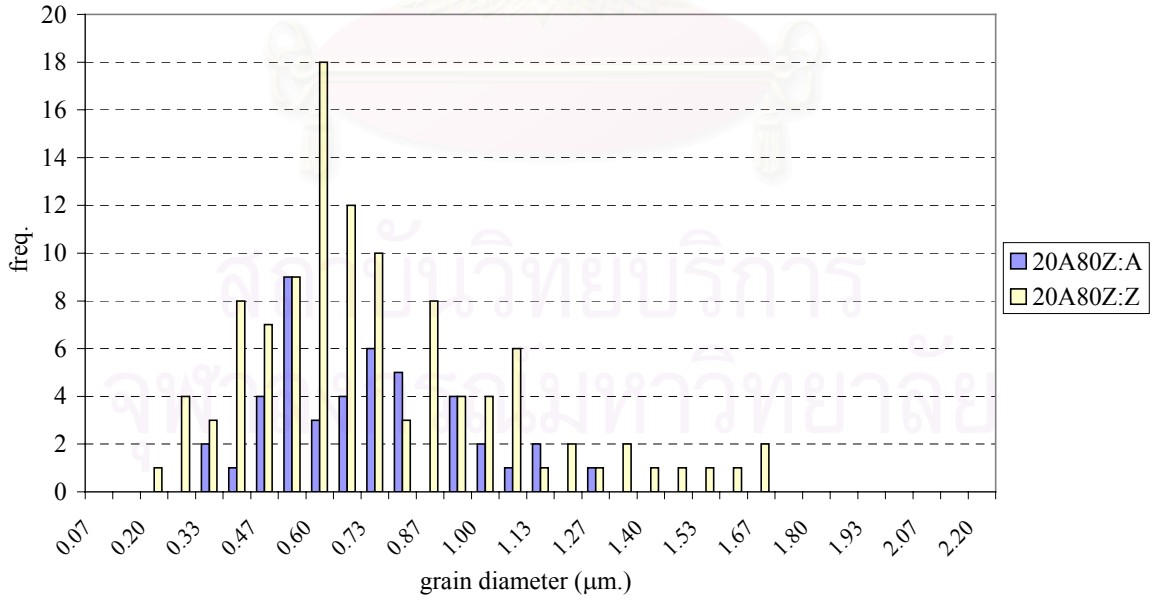
freq.
grain diameter (μm.)
20A80Z:A
20A80Z:Z

Appendix 7

Vickers hardness and fracture toughness of standard samples from Japan.

material	condition	sintering temp.(^{O}C)	relative density (%)	2a (μm)	2c (μm)	H_v (GPa)	STDEV	K_{1c} (MPa.$m^{1/2}$)
ZrO_2 JFCC				120.0	195.6	12.63	0.49	7.1
				119.3	193.0	12.78		7.2
				119.2	187.4	12.80		7.5
				115.2	185.6	13.70		7.4
	average			118.4	190.4	12.98	0.49	7.3
ZrO_2 TOSOH				118.4	236.2	12.97	0.12	5.3
				118.1	234.3	13.04		5.3
				117.6	225.4	13.15		5.6
				118.7	218.8	12.91		5.9
	average			118.2	228.7	13.02	0.12	5.5

Vickers hardness and fracture toughness of pure starting powder specimens.

material	condition	sintering temp.(^{O}C)	relative density (%)	2a (μm)	2c (μm)	H_v (GPa)	STDEV	K_{1c} (MPa.$m^{1/2}$)
ZrO_2 GTYS-5	as-received	1550	93.95	132.4	254.4	10.38	0.42	5.3
				126.5	247.1	11.37		5.3
				129.4	244.1	10.86		5.5
				126.5	248.5	11.37		5.2
	average			128.7	248.5	11.00	0.42	5.3
ZrO_2 GTYS-5	milled used Al_2O_3 balls	1500	94.40	111.8	208.8	14.56	0.63	6.0
				114.7	219.1	13.82		5.7
				117.7	227.9	13.14		5.5
				117.7	201.5	13.14		6.6
	average			115.4	214.3	13.66	0.63	5.9
ZrO_2 GTYS-5	milled used ZrO_2 balls	1500	97.50	125.2	217.6	11.60	0.37	6.3
				125.4	201.0	11.56		7.1
				121.7	202.6	12.28		6.8
				121.4	198.4	12.34		7.0
	average			123.4	204.9	11.95	0.37	6.8
ZrO_2 GTYS-5	milled used ZrO_2 balls	1550	96.00	121.7	211.4	12.28	0.35	6.4
				125.6	218.6	11.53		6.3
				125.0	224.4	11.64		6.0
				124.8	219.8	11.68		6.2
	average			124.3	218.6	11.78	0.35	6.2

Vickers hardness and fracture toughness of composite specimens.

material	condition	sintering temp.(^{O}C)	relative density (%)	2a (μm)	2c (μm)	H_v (GPa)	STDEV	K_{1c} (MPa.$m^{1/2}$)
80A20Z		1600	98.11	104.3	232.5	16.73	0.53	6.5
				106.8	232.3	15.96		6.7
				109.3	282.5	15.24		5.1
				107.0	261.0	15.88		5.6
	average			106.8	252.1	15.95	0.53	6.0
60A40Z		1600	98.03	111.3	274.5	14.69	0.43	5.2
				109.0	287.5	15.31		4.8
				108.8	268.5	15.38		5.3
				109.8	250.0	15.10		5.9
	average			109.7	270.1	15.12	0.43	5.3
40A60Z		1600	97.78	114.8	256.5	13.81	0.42	5.6
				111.3	255.3	14.69		5.4
				114.3	260.0	13.93		5.4
				114.3	242.8	13.93		6.0
	average			113.6	253.6	14.09	0.42	5.6
20A80Z		1600	96.51	122.5	246.0	12.12	0.38	5.8
				119.3	232.5	12.79		6.2
				122.5	240.5	12.12		6.0
				120.5	241.8	12.52		5.9
		average		121.2	240.2	12.39	0.38	6.0

Appendix 8

Example of crack paths for the materials examined [23].

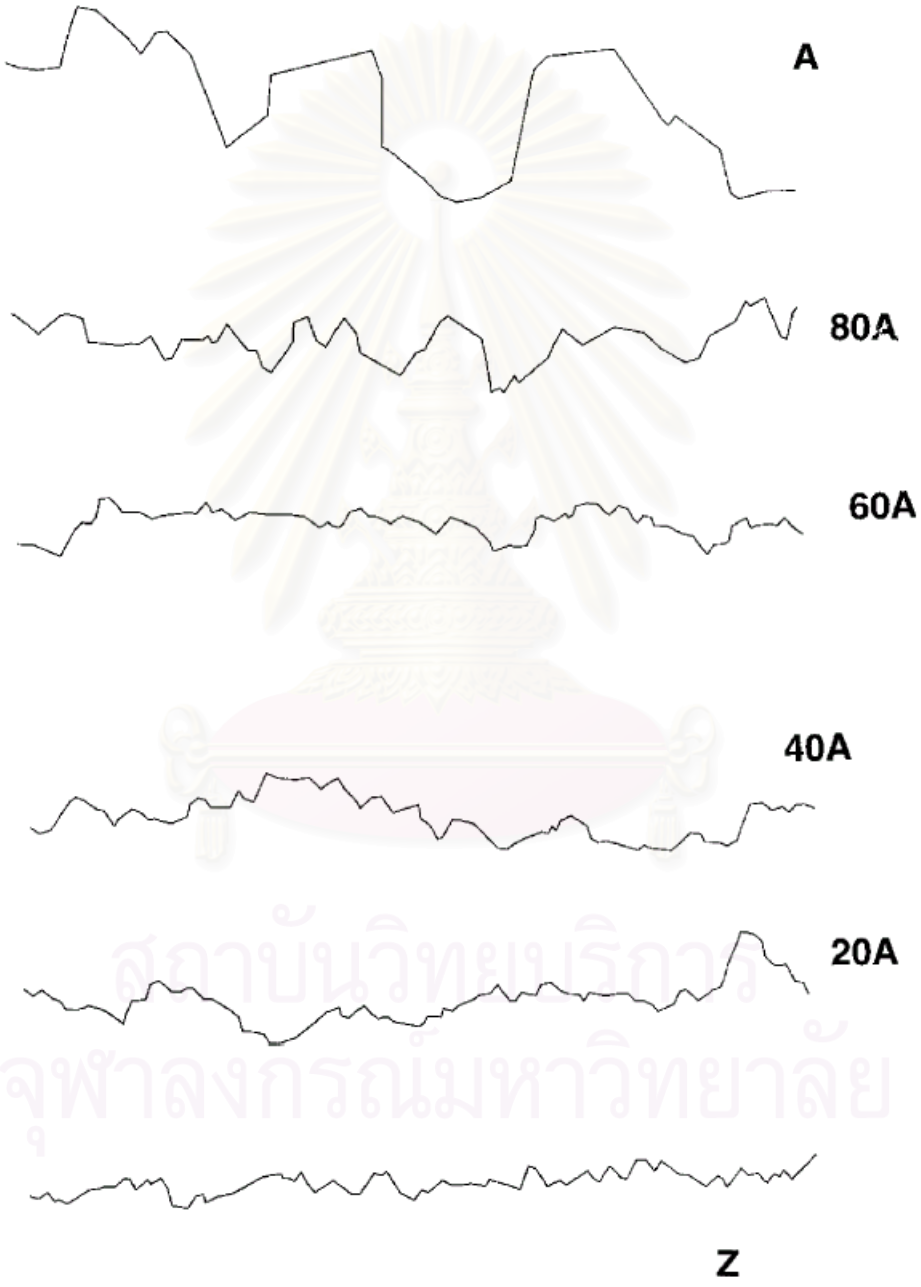

Appendix 9

Detail of specimens for strength measurement.

Conditions	No. Specimen	Thickness (mm)	radius (mm)	x	y	P (N)	Strength (MPa)		
0A100Z 1550^{O}C	1	1.973	14.825	-5.632	1.484	1165	508.3	Max.	579.4
	2	2.486	14.467	-5.571	1.578	1980	546.6		
	3	2.438	14.458	-5.570	1.580	2017	579.4		
	4	1.195	14.433	-5.565	1.587	405.3	484.3	Min.	458.4
	5	1.197	14.442	-5.567	1.584	384.9	458.4		
	6	1.192	14.417	-5.563	1.591	397.9	478.6		
	7	1.189	14.317	-5.545	1.618	456	552.0	Average	513.0
	8	1.198	14.667	-5.605	1.525	446.5	529.9		
	9	1.190	14.458	-5.570	1.580	394.4	475.7		
	10	1.195	14.450	-5.568	1.582	432.2	516.6		
20A80Z 1550^{O}C	1	2.123	14.592	-5.592	1.544	1765	667.4	Max.	678.9
	2	2.115	14.592	-5.592	1.544	1703	648.9		
	3	2.526	14.642	-5.601	1.531	2281	608.7		
	4	2.119	14.642	-5.601	1.531	1550	587.8	Min.	520.0
	5	2.538	14.650	-5.602	1.529	1968	520.0		
	6	2.123	14.600	-5.594	1.542	1745	659.5		
	7	2.124	14.592	-5.592	1.544	1700	642.2	Average	632.3
	8	2.113	14.600	-5.594	1.542	1775	677.2		
	9	2.612	14.608	-5.595	1.540	unbreak			
	10	2.115	14.600	-5.594	1.542	1782	678.9		

Conditions	No. Specimen	Thickness (mm)	radius (mm)	x	y	P (N)	Strength (MPa)		
80A20Z 1500^{O}C	1	2.024	15.650	-5.765	1.281	896.3	368.1	Max.	368.1
	2	1.648	15.658	-5.766	1.279	536.9	332.6		
	3	2.250	15.808	-5.790	1.245	786.2	260.8		
	4	2.042	15.717	-5.776	1.266	637.2	257.0	Min.	253.8
	5	1.633	15.708	-5.774	1.268	537.1	338.6		
	6	1.640	15.675	-5.769	1.275	436.8	273.1		
	7	1.647	15.708	-5.774	1.268	452.2	280.4	average	291.7
	8	1.640	15.775	-5.785	1.252	497.8	310.9		
	9	1.644	15.692	-5.772	1.272	408	253.8		
	10	2.149	15.758	-5.782	1.256	782.2	284.7		
0A100Z 1600^{O}C	1	2.409	14.525	-5.581	1.562	1527	448.7	Max.	620.8
	2	2.422	14.525	-5.581	1.562	2135	620.8		
	3	2.420	14.525	-5.581	1.562	2107	613.6		
	4	2.100	14.517	-5.580	1.564	1493	577.5	Min.	448.7
	5	2.095	14.525	-5.581	1.562	1355	526.5		
	6	2.107	14.525	-5.581	1.562	1514	581.6		
	7	2.090	14.533	-5.583	1.560	1184	462.2	average	541.1
	8	2.099	14.533	-5.583	1.560	1451	561.6		
	9	2.107	14.525	-5.581	1.562	1271	488.4		
	10	2.096	14.542	-5.584	1.558	1366	530.3		

Conditions	No. Specimen	Thickness (mm)	radius (mm)	x	y	P (N)	Strength (MPa)		
20A80Z 1600^{O}C	1	2.558	14.692	-5.609	1.518	2153	560.0	Max.	572.4
	2	2.592	14.617	-5.597	1.538	1832	464.3		
	3	2.623	14.617	-5.597	1.538	unbreak			
	4	2.271	14.725	-5.615	1.510	1522	501.9	Min.	464.3
	5	2.264	14.608	-5.595	1.540	1670	555.0		
	6	2.267	14.617	-5.597	1.538	1606	532.4		
	7	2.247	14.717	-5.613	1.512	1563	526.6	Average	525.3
	8	2.280	14.667	-5.605	1.525	1748	572.4		
	9	2.275	14.625	-5.598	1.536	1541	507.1		
	10	2.269	14.725	-5.615	1.510	1537	507.6		
80A20Z 1600^{O}C	1	2.006	14.683	-5.608	1.520	1193	504.4	Max.	504.4
	2	2.096	14.608	-5.595	1.540	1228	476.2		
	3	2.166	14.625	-5.598	1.536	1075	390.3		
	4	1.655	14.717	-5.613	1.512	494.2	307.1	Min.	307.1
	5	1.648	14.600	-5.594	1.542	536.9	336.7		
	6	1.646	14.608	-5.595	1.540	516.7	324.7		
	7	1.643	14.733	-5.616	1.507	646.2	407.3	Average	392.9
	8	1.634	14.667	-5.605	1.525	678.8	432.5		
	9	1.656	14.617	-5.597	1.538	694.8	431.7		
	10	1.647	14.700	-5.611	1.516	507.7	318.3		

Appendix 10

SEM micrographs of the fractured surface of 100Z (a) sintered at 1550^{O}C, (b) sintered at 1600^{O}C and 80A20Z (c) sintered at 1550^{O}C, (d) sintered at 1600^{O}C.

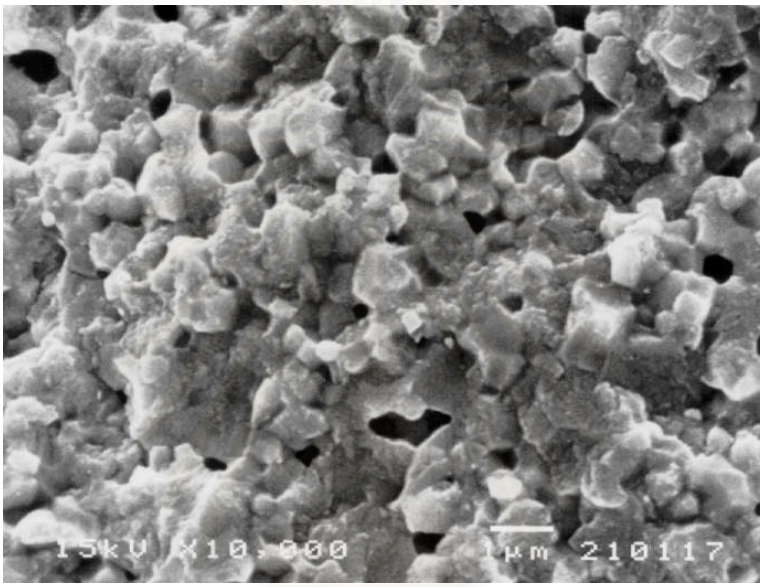

(a)

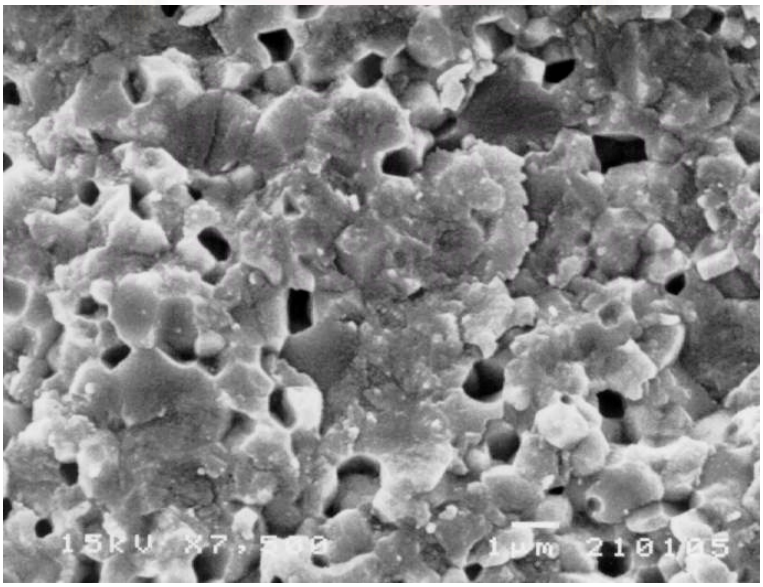

(b)

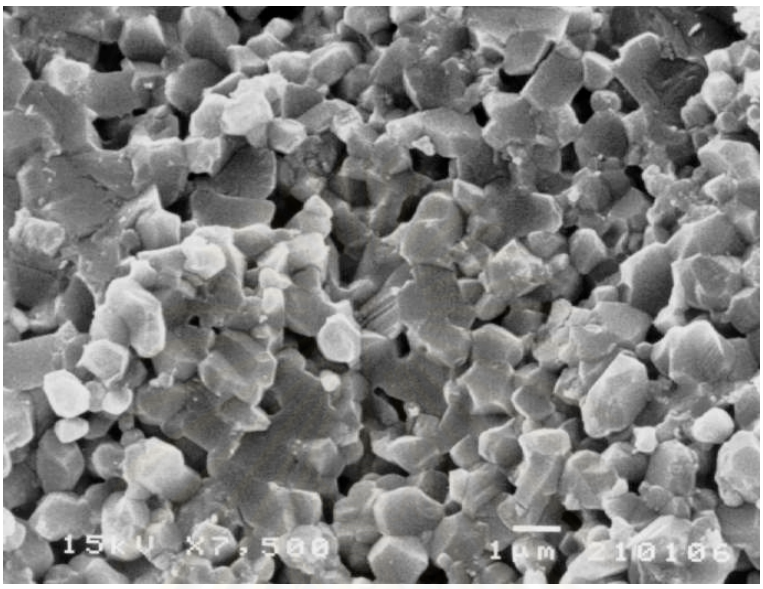

(C)

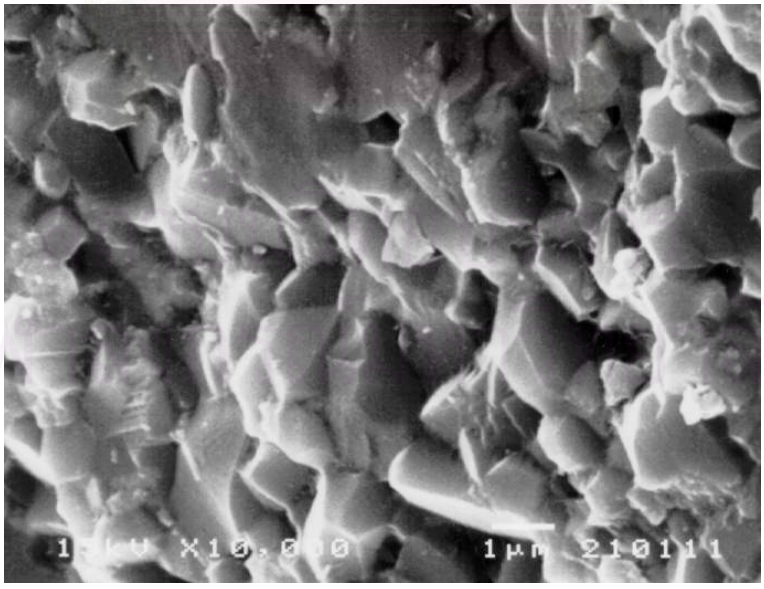

(d)

Appendix 11

Experiment on the composition of Al_2O_3 added with TiO_2.

Table I Percent of theoretical density (%TD) of Al_2O_3 added with TiO_2, mixed by planetary mill, compared with ball mill as a function of sintering temperature.

Sintering temperature (^{O}C)		%TD (Planetary mill)				%TD (Ball mill)			
		1500	1550	1600	1650	1500	1550	1600	1650
Wt% TiO_2	0.2355	91.06	95.94	97.50	97.42	95.33	98.41	98.35	98.20
	0.7907	97.77	97.72	97.70	97.47	98.63	98.28	97.87	97.47
	1.5977	98.00	97.42	97.21	96.85	98.32	97.63	97.01	96.76
	4.1640	97.71	97.21	96.58	96.12	97.77	97.45	97.03	96.07

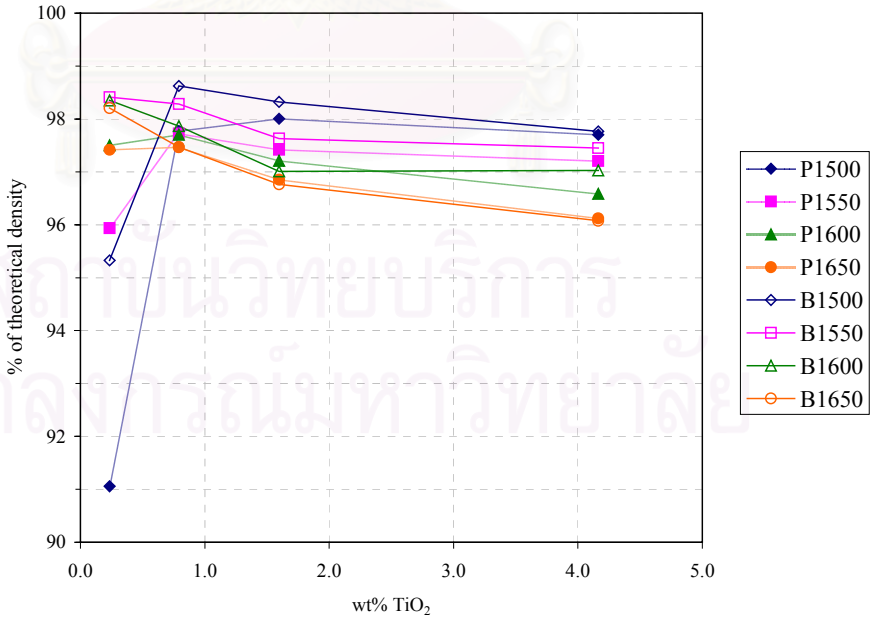

Fig.I Percent of theoretical density (%TD) of Al_2O_3 added with TiO_2. P is planetary mill, B is ball mill.

Experiment on the Al_2O_3-ZrO_2 composite added with TiO_2.

Table II Percent of theoretical density (%TD) of 80A20Z added with 0.2355 wt% TiO_2, mixed by ball mill, as a function of sintering temperature.

Sintering temp. (^{O}C)	W_{sus} (g)	W_{sat} (g)	W_d (g)	%water absorption	Density (g/cm^3)	%TD	% linear shrinkage
1500	2.1806	2.9101	2.9028	0.25	3.97	93.52	19.50
	2.1745	2.9014	2.9014	0.00	3.98	93.81	19.25
	2.1612	2.8839	2.8839	0.00	3.98	93.79	19.25
average	2.1721	2.8985	2.8960	0.08	3.97	93.70	19.33
1550	2.1864	2.8887	2.8872	0.05	4.09	96.57	15.25
	2.1952	2.8995	2.8978	0.06	4.10	96.65	15.25
	2.1889	2.8898	2.8881	0.06	4.10	96.79	15.25
average	2.1902	2.8927	2.8910	0.06	4.10	96.67	15.25
1600	2.2027	2.8924	2.8916	0.03	4.18	98.51	20.50
	2.1962	2.8851	2.8832	0.07	4.17	98.34	20.75
	2.1883	2.8752	2.8726	0.09	4.17	98.26	20.75
average	2.1957	2.8842	2.8825	0.06	4.17	98.37	20.67
1650	2.1980	2.8907	2.8890	0.06	4.16	98.00	20.50
	2.1997	2.8917	2.8912	0.02	4.16	98.17	20.50
	2.1896	2.8824	2.8810	0.05	4.14	97.71	20.50
average	2.1958	2.8883	2.8871	0.04	4.15	97.96	20.50

Table III Percent of theoretical density (%TD) of 60A40Z added with 0.2355 wt% TiO_2, mixed by ball mill, as a function of sintering temperature.

Sintering temp. (^{O}C)	W_{sus} (g)	W_{sat} (g)	W_d (g)	% water absorption	Density (g/cm^3)	%TD	% linear shrinkage
1500	2.2423	2.9122	2.9103	0.07	4.33	90.06	20.70
	2.2338	2.8974	2.8956	0.06	4.35	90.46	20.70
	2.2313	2.8948	2.8931	0.06	4.35	90.39	20.70
average	2.2358	2.9015	2.8997	0.06	4.34	90.30	20.70
1550	2.2605	2.9111	2.9092	0.07	4.45	92.65	21.45
	2.2525	2.9020	2.9002	0.06	4.45	92.52	21.25
	2.2498	2.8977	2.8967	0.03	4.45	92.63	21.25
average	2.2543	2.9036	2.9020	0.05	4.45	92.60	21.32
1600	2.2677	2.9158	2.9145	0.04	4.48	93.20	21.50
	2.2692	2.9171	2.9152	0.07	4.48	93.25	21.25
	2.2574	2.9019	2.9005	0.05	4.48	93.27	21.25
average	2.2648	2.9116	2.9101	0.05	4.48	93.24	21.33
1650	2.2529	2.9048	2.9039	0.03	4.44	92.32	21.00
	2.2728	2.9291	2.9284	0.02	4.45	92.48	21.00
	2.2436	2.8916	2.8913	0.01	4.45	92.47	20.75
average	2.2564	2.9085	2.9079	0.02	4.44	92.42	20.92

Table IV Percent of theoretical density (%TD) of 40A60Z added with 0.2355 wt% TiO_2, mixed by ball mill, as a function of sintering temperature.

Sintering temp. (^{O}C)	W_{sus} (g)	W_{sat} (g)	W_d (g)	% water absorption	Density (g/cm^3)	%TD	% linear shrinkage
1500	2.2895	2.8909	2.8891	0.06	4.79	96.38	21.75
	2.2967	2.8985	2.8969	0.06	4.80	96.57	21.50
	2.2918	2.8949	2.8920	0.10	4.78	96.20	21.75
average	2.2927	2.8948	2.8927	0.07	4.79	96.39	21.67
1550	2.3080	2.9047	2.9032	0.05	4.85	97.56	22.19
	2.3081	2.9028	2.9018	0.03	4.86	97.84	22.19
	2.2993	2.8927	2.8910	0.06	4.85	97.69	22.00
average	2.3051	2.9001	2.8987	0.05	4.85	97.70	22.13
1600	2.2961	2.8913	2.8898	0.05	4.84	97.38	22.00
	2.3207	2.9216	2.9208	0.03	4.84	97.49	22.00
	2.3186	2.9190	2.9184	0.02	4.84	97.50	22.00
average	2.3118	2.9106	2.9097	0.03	4.84	97.46	22.00
1650	2.2990	2.9072	2.9070	0.01	4.76	95.87	21.50
	2.2985	2.9069	2.9062	0.02	4.76	95.81	21.50
	2.3090	2.9200	2.9197	0.01	4.76	95.85	21.50
average	2.3022	2.9114	2.9110	0.01	4.76	95.84	21.50

Table V Percent of theoretical density (%TD) of 20A80Z added with 0.2355 wt% TiO_2, mixed by ball mill, as a function of sintering temperature.

Sintering temp. (^{O}C)	W_{sus} (g)	W_{sat} (g)	W_d (g)	% water absorption	Density (g/cm^3)	%TD	% linear shrinkage
1500	2.3015	2.8353	2.8341	0.04	5.29	97.33	23.00
	2.3167	2.8526	2.8512	0.05	5.30	97.53	23.00
	2.3110	2.8469	2.8444	0.09	5.29	97.30	23.00
average	2.3097	2.8449	2.8432	0.06	5.29	97.39	23.00
1550	2.3178	2.8513	2.8507	0.02	5.32	98.01	23.00
	2.3326	2.8704	2.8696	0.03	5.32	97.87	22.75
	2.3205	2.8568	2.8562	0.02	5.31	97.68	23.00
average	2.3236	2.8595	2.8588	0.02	5.32	97.85	22.92
1600	2.2868	2.8283	2.8273	0.04	5.20	95.72	22.50
	2.3261	2.8746	2.8734	0.04	5.22	96.04	22.50
	2.3364	2.8862	2.8855	0.02	5.23	96.21	22.50
average	2.3164	2.8630	2.8621	0.03	5.22	95.99	22.50
1650	2.3208	2.8873	2.8869	0.01	5.08	93.42	21.75
	2.3214	2.8891	2.8886	0.02	5.07	93.28	21.75
	2.3023	2.8646	2.8639	0.02	5.07	93.37	21.75
average	2.3148	2.8803	2.8798	0.02	5.07	93.36	21.75

Table VI Percent of theoretical density (%TD) of Al_2O_3-ZrO_2 added with 0.2355 wt% TiO_2, mixed by ball mill, as a function of sintering temperature.

composite	Sintering temp. (^{O}C)	Density (g/cm^3)	%TD
100AT	1500	3.77	95.33
	1550	3.89	98.41
	1600	3.88	98.35
	1650	3.88	98.20
80A20ZT	1500	3.97	93.70
	1550	4.10	96.67
	1600	4.17	98.37
	1650	4.15	97.96
60A40ZT	1500	4.34	90.30
	1550	4.45	92.60
	1600	4.48	93.24
	1650	4.44	92.42
40A60ZT	1500	4.79	96.39
	1550	4.85	97.70
	1600	4.84	97.46
	1650	4.76	95.84
20A80ZT	1500	5.29	97.39
	1550	5.32	97.85
	1600	5.22	95.99
	1650	5.07	93.36

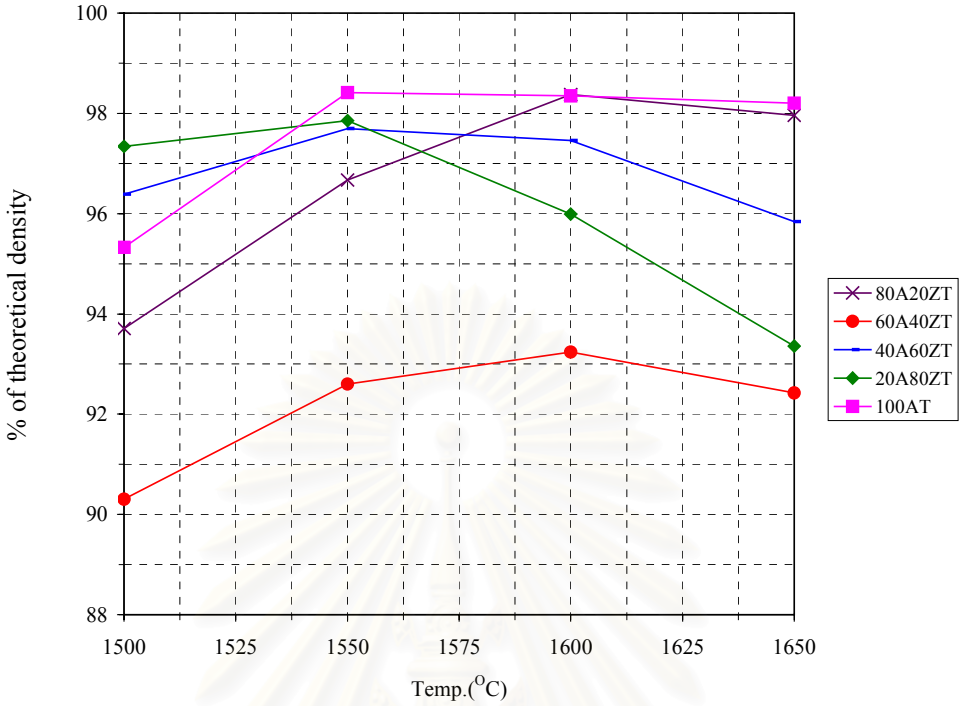

Fig.II Percent of theoretical density (%TD) of Al_2O_3-ZrO_2 added with 0.2355 wt% TiO_2 as a function of sintering temperature.

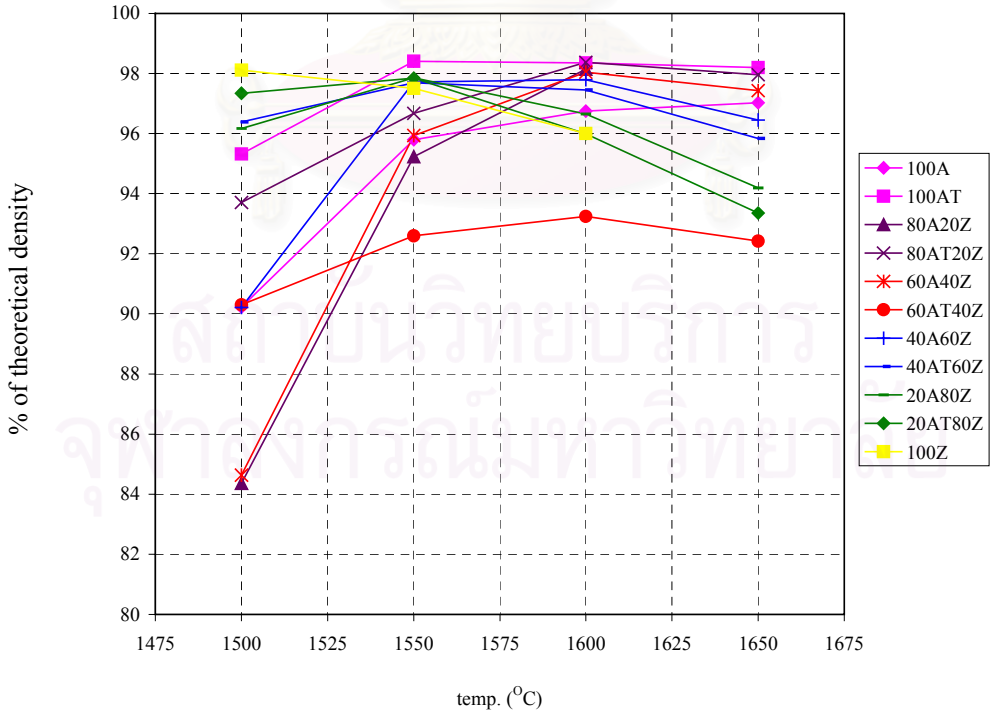

Fig.III Comparison of the percent of theoretical density (%TD) between Al_2O_3-ZrO_2 and Al_2O_3-ZrO_2 added with 0.2355wt% TiO_2 as a function of sintering temperature.

Vickers hardness and fracture toughness of composites specimens added with 0.2355wt% TiO_2.

material	condition	sintering temp.(^{O}C)	relative density (%)	2a (μm)	2c (μm)	H_v (GPa)	STDEV	K_{1c} (MPa.$m^{1/2}$)
80A20ZT		1600	98.37	110.0	302.0	15.03	0.34	4.7
				108.4	256.8	15.48		5.9
				111.6	307.5	14.60		4.7
				110.4	300.0	14.92		4.8
	average			110.1	291.6	15.01	0.34	5.0
60A40ZT		1600	93.24	119.1	291.3	12.82	0.55	5.1
				114.6	287.5	13.85		5.0
				114.4	288.0	13.90		5.0
				119.1	286.0	12.82		5.2
	average			116.8	288.2	13.35	0.55	5.1
40A60ZT		1600	97.46	120.0	261.8	12.63	0.00	5.6
				120.0	258.5	12.63		5.8
				120.0	254.3	12.63		5.9
				120.0	250.0	12.63		6.1
	average			120.0	256.1	12.63	0.00	5.8
20A80ZT		1600	95.99	124.6	262.5	11.71	0.08	5.4
				124.8	276.0	11.68		5.0
				124.9	272.5	11.66		5.1
				125.7	260.8	11.51		5.5
		average		125.0	267.9	11.64	0.08	5.2

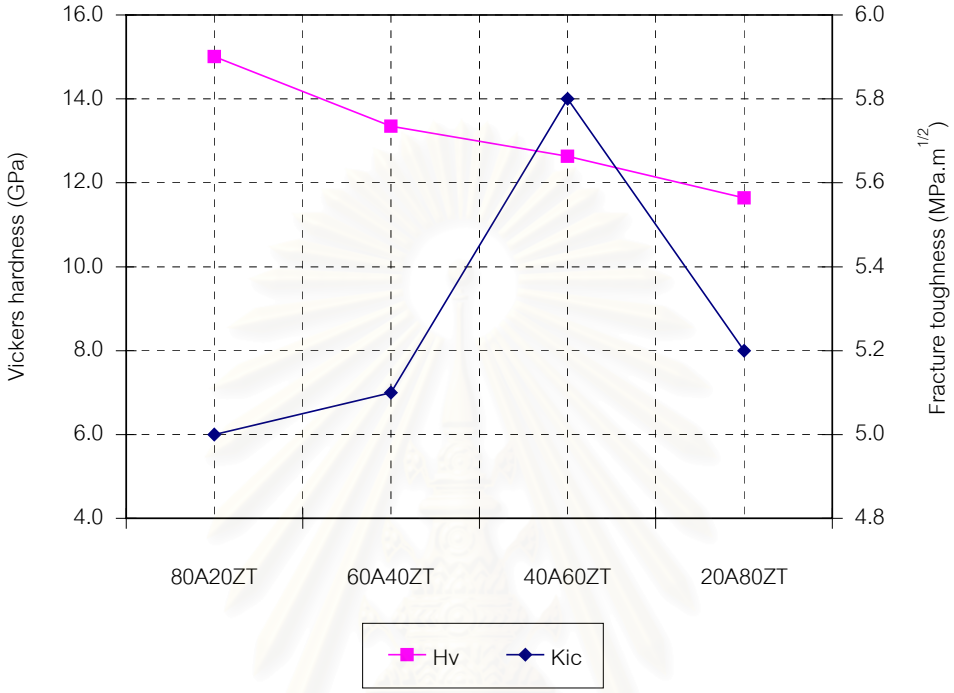

Fig.IV Relationship of Vickers hardness and fracture toughness of Al_2O_3-ZrO_2 added with 0.2355wt% TiO_2.

Appendix 12

The experiment on the flexural strength of 20A80Z(JIS R1601)

temp.(^{O}C)	group	specimen no.	thickness (mm)	width (mm)	load P (N)	strength s (MPa)	$s_{avr.}$ (MPa)	SD.
1500	A	1	3.05	4.00	657.2	529.9	500.6	41.3
		2	3.05	4.00	584.7	471.4		
		3	3.05	4.00	325.0	262.0		
	B	1	3.00	4.00	587.4	489.5	444.0	36.8
		2	3.10	4.00	582.0	454.2		
		3	3.05	4.00	496.1	400.0		
		4	3.05	4.00	574.2	462.9		
		5	3.05	4.00	512.8	413.4		
	C	1	3.05	4.00	562.1	453.2	471.1	17.4
		2	3.05	4.00	612.9	494.1		
		3	3.05	4.00	215.2	173.5		
		4	3.05	4.00	587.1	473.3		
		5	3.05	4.00	575.3	463.8		

temp.(^{O}C)	group	specimen no.	thickness (mm)	width (mm)	load P (N)	strength s (MPa)	$s_{avr.}$ (MPa)	SD.
1550	A	1	3.05	4.00	602.7	485.9	494.7	19.7
		2	3.05	4.00	596.5	480.9		
		3	3.05	4.00	641.6	517.3		
	B	1	3.10	4.00	523.2	408.3	449.0	46.6
		2	3.10	4.00	527.5	411.7		
		3	3.05	4.00	609.1	491.1		
		4	3.05	4.00	529.4	426.8		
		5	3.05	4.00	629.0	507.1		
	C	1	3.10	4.00	623.1	486.3	474.2	34.7
		2	3.05	4.00	579.6	467.3		
		3	3.05	4.00	623.1	502.4		
		4	3.05	4.00	617.7	498.0		
		5	3.05	4.00	517.3	417.1		

temp.(°C)	group	specimen no.	thickness (mm)	width (mm)	load P (N)	strength s (MPa)	$s_{avr.}$ (MPa)	SD.
1600	A	1	3.05	4.00	704.4	567.9	566.3	15.4
		2	3.05	4.00	682.4	550.2		
		3	3.05	4.00	720.5	580.9		
	B	1	3.05	4.00	600.0	483.7	496.6	35.4
		2	3.05	4.00	689.4	555.8		
		3	3.05	4.00	619.6	499.5		
		4	3.05	4.00	595.2	479.9		
		5	3.05	4.00	575.6	464.1		
	C	1	3.05	4.00	688.6	555.2	564.1	23.7
		2	3.05	4.00	742.0	598.2		
		3	3.00	4.00	670.9	559.1		
		4	3.05	4.00	674.4	543.7		
		5	3.05	4.00	757.6	610.8		

◆ Group A : non polished surface, heat treatment 1200OC, 1 h

■ Group B : polished surface, heat treatment 1200OC, 1 h

▲ Group C : polished surface

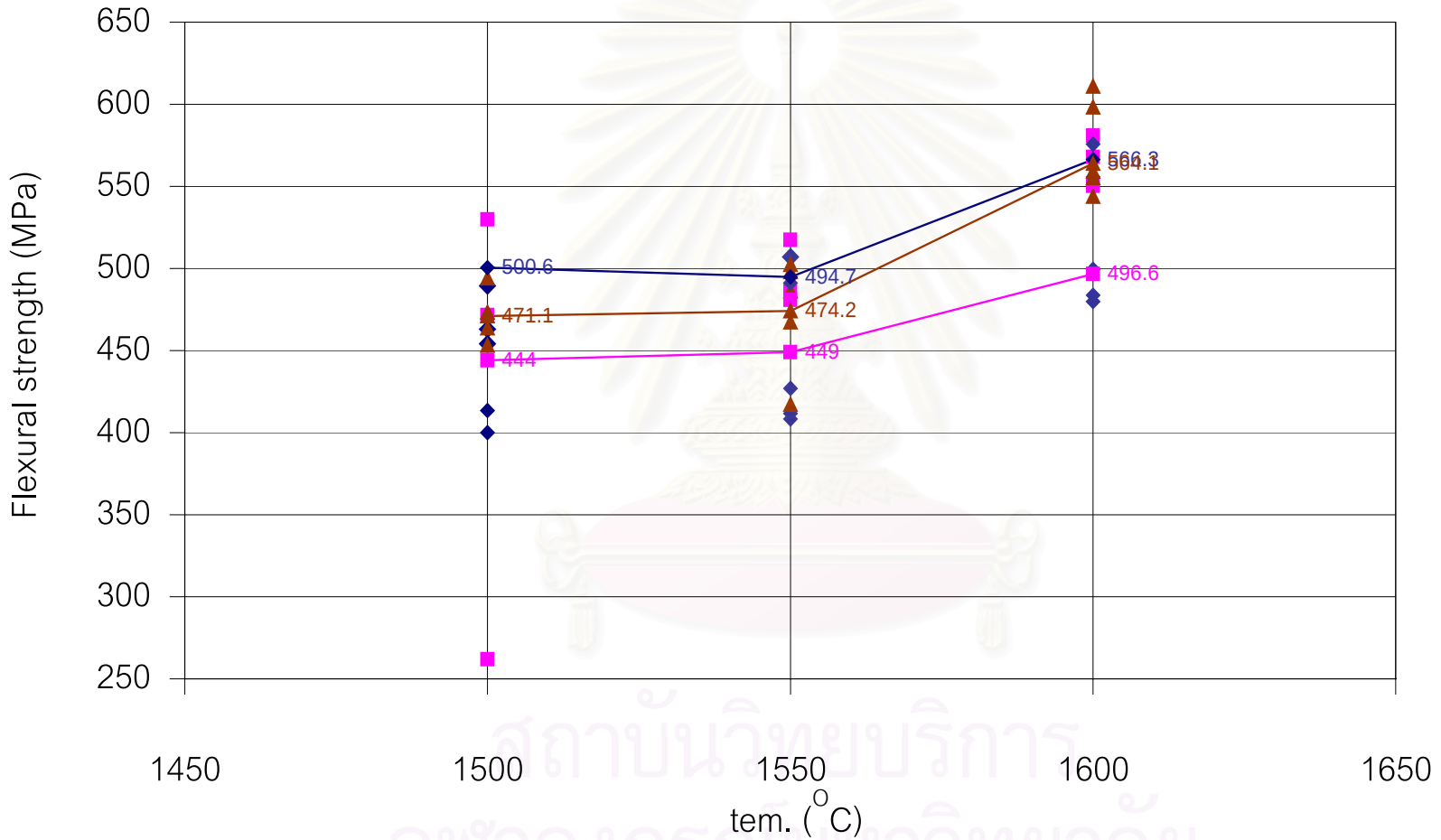

Fig.V Relationship of flexural strength and sintering temperature of 20A80Z (JIS R1601) ◆ Group A, ■ Group B, and ▲ Group C

BIOGRAPHY

Miss Khanthima Hemra was born on the 17th of August 1979, in Roi-Et. After graduating with a Bachelor's Degree in Materials Science from the Department of Physics, Faculty of Science, Chiang Mai University in May 2001, she continued a further study in Master's Degree in the field of Ceramic Technology at Chulalongkorn University and graduated in May 2004.